Optimal Configuration of a Convection-Permitting Regional Climate Model in Simulating Precipitation Extremes: The Saguenay Flood

SOUMIK GHOSH,[a,b] PHILIPPE LUCAS-PICHER,[a,b] PHILIPPE ROY,[a,c] PHILIPPE GACHON,[a,d] AND ALEJANDRO DI LUCA[a,b]

[a] *Étude et Simulation du Climat à l'Échelle Régionale (ESCER) Center, Université du Québec à Montréal, Montréal, Québec, Canada*
[b] *Department of Earth and Atmospheric Sciences, Université du Québec à Montréal, Montréal, Québec, Canada*
[c] *Centre de Recherche d'Hydro-Québec, Montréal, Québec, Canada*
[d] *Department of Geography, Université du Québec à Montréal, Montréal, Québec, Canada*

(Manuscript received 24 January 2025, in final form 22 September 2025, accepted 6 October 2025)

ABSTRACT: This case study concerns a major flood event occurred in July 1996 in the Saguenay region (Québec, Canada) induced by heavy and persistent rainfall over this river basin. Various configurations of the CRCM6/Global Environmental Multiscale (GEM) model, version 5 (GEM5), regional climate model (RCM) using 12-km (0.11° × 0.11°) and convection-permitting (CP) 2.5-km (0.0225° × 0.0225°) resolutions are used to evaluate added value from CP simulations on the simulated extreme precipitation characteristics. The effects of spectral nudging (SN) and initial soil moisture conditions (ISMCs) on surface are also tested on the simulated rainfall. The evaluation of all simulations shows a significant improvement in reproducing precipitation extremes with the CP model (CPM) at 2.5 km and substantial influences from SN and ISMCs. The SN in the CP simulation improved the spatial and temporal patterns of precipitation extremes. Additionally, forced ISMC from long-term simulations at a 12-km resolution significantly enhanced the model's ability to capture rainfall intensity, using rainfall observed stations as a reference dataset. This research contributes to the understanding of extreme precipitation events and their reliability as simulated by various configurations of our RCM, and the need to apply higher resolution and accurate surface conditions in the CRCM6/GEM5 for future projections, and their use in design infrastructures and flood risk management strategies.

KEYWORDS: Convection; Extreme events; Precipitation; Soil moisture; Climate models; Flood events

1. Introduction

Climate change poses a significant challenge to socioeconomic development, including the achievement of sustainable development goals [SDGs; see the last United Nations Department of Economic and Social Affairs (2024) report] in connection with the intensification and increased frequency of extreme rainfall events. The Sixth Assessment Report (AR6) of the Intergovernmental Panel on Climate Change (IPCC) emphasizes that rising temperatures increase atmospheric moisture content, intensifying the water cycle, leading to more extreme precipitation and persistence of dry events, which result in heightened risks of increased flooding and more severe droughts (IPCC 2023), respectively. In Canada, these impacts are particularly pronounced, as evidenced by changing precipitation patterns (Bush and Lemmen 2019), human-influenced floods (Gillett et al. 2022), and flood occurrences and duration over eastern Canada (see Burn and Whitfield 2016; Benoit et al. 2022). Extreme rainfall events and their effects on flood occurrences, such as the devastating one in Alberta in June 2013 (Teufel et al. 2017), in British Columbia in 2021 (Gillett et al. 2022), and in the Saguenay region of Quebec in July 1996 [Environment and Climate Change Canada (ECCC) 1997; Lin et al. 2002] and in 2017 and 2019 during spring over the Ottawa River basin (Benoit et al. 2022), are leaving lasting impacts on communities, infrastructure, and ecosystems across the country (Warren and Lulham 2021). With climate models projecting further increases in extreme precipitation under continued greenhouse gas emissions (IPCC 2023), an improved projection of flood features at the basin scale associated with regional and local extreme rainfall is crucial for building resilience in Canada and beyond. This needs to be done with high-resolution climate modeling tools, as precipitation extremes for both process understanding and modeling and flood risk management require high temporal and spatial resolution (e.g., Gutowski et al. 2020) including convective storm environment responsible for heavy rainfall (see Prein et al. 2015). In fact, high-resolution simulations with regional convection-permitting (CP) models (CPMs) allow to explicitly resolve convection and have a better representation of orography, leading to a more accurate representation of the spatial occurrence, amounts, and diurnal cycle of heavy precipitation, clouds, snow, and local winds than coarse-scale models (Belušić et al. 2018; Lüthi et al. 2019; Hentgen et al. 2019; Ban et al. 2021; Pichelli et al. 2021).

The introduction of CPMs in the early 2010s represents a crucial step forward in addressing some of the limitations inherent in coarse-scale climate models. These finer resolution models offer a significant improvement in accuracy and detail (convective processes, topography, etc.), leading to more precise simulations and, consequently, better projection of climate extremes and

Denotes content that is immediately available upon publication as open access.

Supplemental information related to this paper is available at the Journals Online website: https://doi.org/10.1175/JHM-D-25-0011.s1.

Corresponding author: Soumik Ghosh, ghosh.soumik@uqam.ca, soumik.ghosh@fulbrightmail.org

DOI: 10.1175/JHM-D-25-0011.1

flood risk assessments (Prein et al. 2015; Lucas-Picher et al. 2021). The progress and prospects of high-resolution climate modeling have been emphasized, highlighting its potential to upgrade our approach to climate research (Schär et al. 2016). CPMs can be instrumental in assessing the localized impacts of climate change on water resources, as exemplified in their case study in the western United States from Rasmussen et al. (2011). Integrating CPMs into the climate modeling framework could offer further refinement in revisiting extreme precipitation events, by enhancing the accuracy of our climate projections understanding and bolstering resilience to the escalating challenges posed by climate change–induced extreme weather (Fosser et al. 2024).

CPMs present in principle some added value in the understanding of localized climate processes, providing unprecedented resolution that captures fine-scale weather phenomena such as convection, cloud formation, and topographically induced weather patterns (e.g., Schär et al. 2020; Pichelli et al. 2021; Fosser et al. 2024). However, accurately simulating extreme weather events within these models still requires nudging from the large-scale fields to the regional climate model (RCM). Spectral nudging (SN) helps ensure that the large-scale conditions in the RCM closely match those of the driving data, bringing the RCM's large-scale patterns closer to real-world conditions when using reanalysis data (von Storch et al. 2000; Miguez-Macho et al. 2004; Lucas-Picher et al. 2008). It has been shown to improve the simulation of precipitation and temperature patterns, emphasizing better adherence to large-scale climate dynamics (Rockel and Geyer 2008; Miguez-Macho et al. 2005). This nudging technique enhances the representation of storm tracks and the frequency and intensity of extreme weather events by maintaining the integrity of large-scale atmospheric flow within the regional domain of simulation (Tang et al. 2018; Bowden et al. 2012; Feser and Barcikowska 2012).

In this context, the Aleas, Risques et Résilience des Infrastructures Minières et Électriques (ARRIMÉ) project has been initiated. This 5-yr initiative (2023–28) aims at understanding and projecting the changes in probable maximum precipitation and extreme flood hazards to prevent deleterious impacts on human health and safety, hydroelectric power infrastructures and their integrity, and mine industries under a partnership with Hydro-Québec, industrial partners in the mining sector of the Institute for Mining and Environment Research [IRME, at Université du Québec en Abitibi-Témiscamingue (UQAT)-Polytechnique], Ouranos, and the Ministère de l'Environnement et de la Lutte contre les Changements Climatiques, de la Faune et des Parcs (MELCCFP) of Québec. As part of the ARRIMÉ project, the current study focuses on weather extremes over the Québec region and emphasizes the added value of using CPM simulations. This study identifies an optimal configuration at the CP scale, focusing on the simulation of weather extremes analyses with the Canadian RCM, version 6 (CRCM6), which is based on the Global Environmental Multiscale (GEM) Model, version 5.1.1 (GEM5.1.1; McTaggart-Cowan et al. 2019) (hereafter CRCM6/GEM5), and leverages an ensemble of high-resolution climate model projections. The findings of this project are expected to inform effective climate adaptation and mitigation strategies and infrastructure design, contributing to the development of more resilient infrastructures.

Addressing the limitations of current climate models is crucial for improving our understanding and projection of climate change impacts, particularly concerning extreme events (e.g., Takayabu et al. 2022). The province of Québec, Canada, where the ARRIMÉ project focuses, holds critical importance for managing infrastructure security and mine waste management in the face of climate and weather extremes. Changes in precipitation and temperature patterns are impacting streamflow, which is critical for hydropower, potentially reducing its reliability on security and efficiency (Hydro-Québec 2022). Additionally, extreme weather events can damage infrastructure and disrupt power distribution (Hydro-Québec 2022). Mine waste management is also threatened by increased rainfall and flooding, which can lead to contamination of local water sources. This contamination poses significant risks to ecosystems and communities dependent on these water sources (Asif and Chen 2016). Addressing these challenges requires robust climate models capable of accurately simulating extreme weather events with more accuracy.

Therefore, to advance the precision of modeling extreme rainfall events, this study focuses on identifying an optimal configuration for the CRCM6/GEM5 RCM to assess the added value of CPM simulations for analyzing climate extremes in Québec, Canada. The Saguenay 1996 flood and extreme precipitation event, one of the most catastrophic in Canadian history, resulted in widespread flooding and significant socioeconomic impacts and is being examined for this specific purpose. During this event, most weather stations over the Saguenay area measured an amount of 175–300 mm of rainfall in only 2 days (19–20 July 1996), which constitutes an unprecedented record for July using the available historical time series of precipitation from observed data of ECCC (2024). One key aspect of this study is to apply the added value of employing a higher resolution of 2.5 km compared to a 12-km resolution, as this can significantly enhance the model's ability to simulate small-scale features that are important in extreme events, which often occur at the local scale. Additionally, the significance of driving strategies (with and without SN) in enhancing the performance of RCMs for this study of case study is crucial, particularly for simulating extreme events. Soil moisture, identified as a crucial factor and highly sensitive in simulating rainfall patterns within reliable regional climate projections (Endris et al. 2013; Wei et al. 2016), is thoroughly assessed in this study due to its demonstrated impact on rainfall pattern simulation and moisture flux.

2. Study area, data, and methods

a. Study area: Main features and description of the case study

The Saguenay River located in Quebec, Canada, is home to numerous large water reservoirs that play a pivotal role in hydroelectric power generation. On 19 and 20 July 1996, relentless heavy rains quickly saturated the ground and stands out as one of Canada's most devastating natural disasters (ECCC 1997; Milbrandt and Yau 2001). The early stage of storm development (1800 UTC 19 July 1996) shows a moderate low pressure system [using mean sea level pressure (MSLP)] and

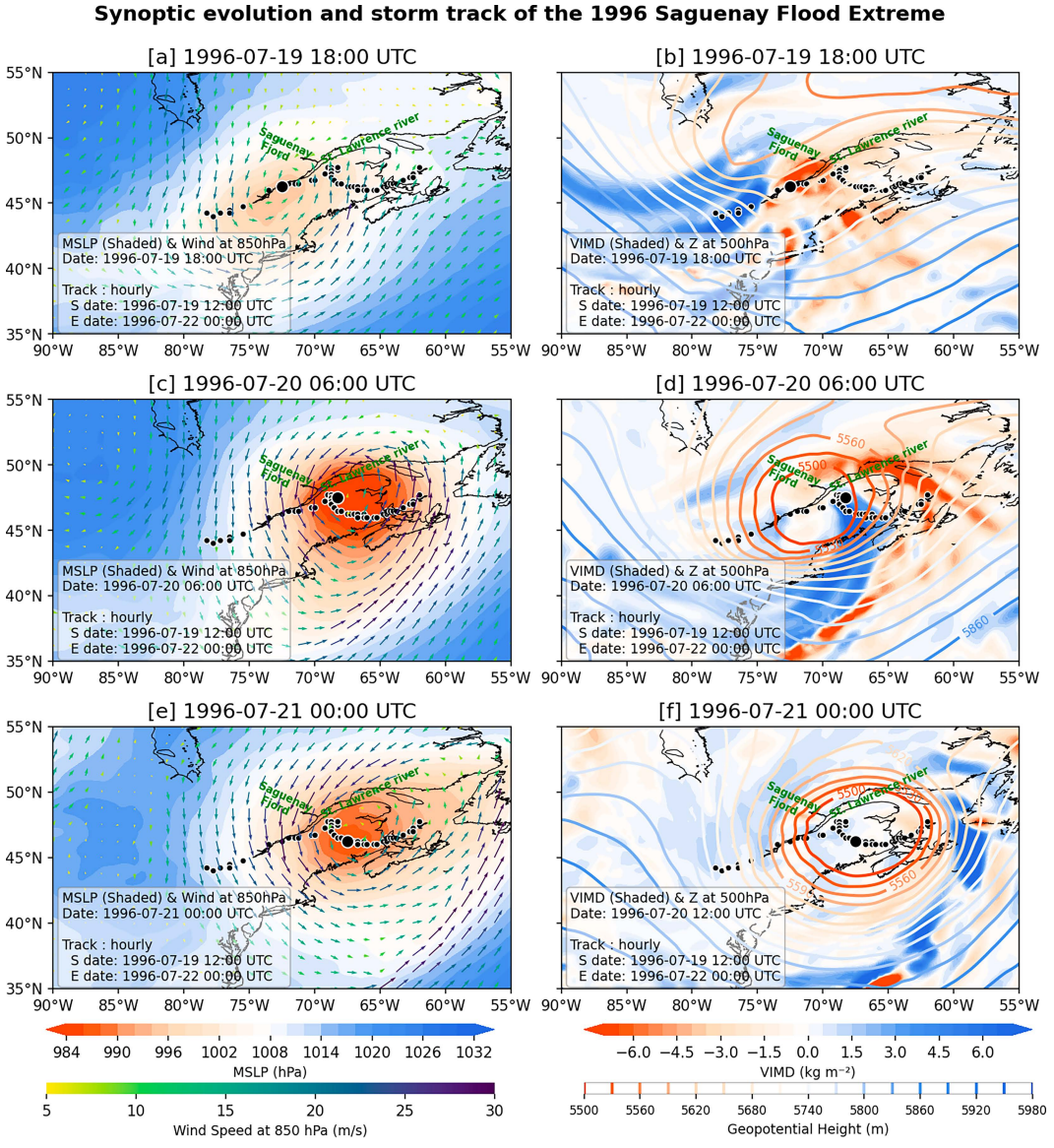

FIG. 1. Synoptic storm-track features at (a),(b) 1800 UTC 19 Jul, (c),(d) 0600 UTC 20 Jul, and (e),(f) 0000 UTC 21 Jul 1996 based on ERA5 reanalysis data. (a),(c),(e) MSLP (hPa) and 850-hPa wind vectors (m s^{-1}). (b),(d),(f) VIMD (kg m^{-2}) and 500-hPa geopotential height (m). The storm track is overlaid in each panel using hourly minimum MSLP points from 1200 UTC 19 Jul to 0000 UTC 22 Jul. The large black point in each panel indicates the storm's position at the respective hour of that panel.

is associated with wind fields at 850 hPa, with moisture convergence [negative vertically integrated moisture divergence (VIMD)] intensifying over southeastern Canada (Figs. 1a,b). Storm reaches peak intensity during 0600 UTC 20 July 1996, with a deep low (MSLP $<$ 984 hPa) centered over the Saint Lawrence River region (approximately 47.75°N, 68.25°W). Strong cyclonic winds (>30 m s^{-1} on the west and east sides of the storm) at 850 hPa and large-scale moisture convergence over the western part of the storm have the potential to trigger intense precipitation (Figs. 1c,d). In fact, the large-scale moisture divergence (positive value of VIMD) is present in the western and southern parts of the storm, and moisture convergence (negative value of VIMD) is present in the west of the storm center and in the eastern and northeastern parts of the storm, during 0600 UTC 20 July. These two features of VIMD with a sharp gradient of humidity or horizontal moisture flux (integrated over all pressure levels) have the potential to trigger intense precipitation in the west and in the north of the storm location. In other words, the frontal zone, characterized by a strong moisture gradient, induces upward vertical motion. Combined with the horizontal advection of moisture and enhanced convergence (as indicated by negative VIMD), this leads to intense precipitation to the west and north of the storm center (Funk 2011). After a few hours, the

TABLE 1. Weather station information summary.

Station name	Latitude (°N)	Longitude (°W)	Elevation (m)	Climate ID	WMO ID
Apica	47.93	71.38	—	—	—
Lac-Ha! Ha!	47.98	70.78	502.90	7063647	—
Rivière-Aux-Écorces	48.18	71.65	—	—	—
Bagotville A	48.33	71.00	159.10	7060400	71727
Cap-Éternité	48.25	70.40	—	—	—
Portage-Des-Roches	48.30	71.22	164.60	7066080	—

storm starts to weaken slightly and move toward the east (0000 UTC 21 July 1996) and MSLP shows < 980 hPa. However, VIMD fields show continued moisture convergence from the ocean and Saint Laurent Gulf (Figs. 1e,f), ultimately contributing to the extreme precipitation and subsequent flooding observed. The disaster resulted in multiple fatalities, the evacuation of over 16 000 residents (Maltais et al. 1999), and more than $1 billion in damages (Faucher 2002). The event exposed critical vulnerabilities in flood management and infrastructure (Tremblay and Guillaud 2019), highlighting the urgent need for improved prevention and preparedness measures.

b. Data and experimental setup

1) OBSERVED, GRIDDED, AND REANALYSIS DATA

To compare the model simulations presented in the following section, and to comprehend the spatial patterns of precipitation fields over the study area, we employ gridded rainfall data from the ERA5-Land reanalysis at a 9-km resolution (Muñoz-Sabater et al. 2021) and the Regional Deterministic Reforecast System, version 2.1 (RDRS v2.1), at a 10-km resolution (Gasset et al. 2021). Additionally, we use MSLP, geopotential height Z, VIMD, the u- and v-wind components, vertical velocity ω, specific humidity q, and temperature from the ERA5 reanalysis, which has a horizontal resolution of 31 km. All datasets are available at an hourly time scale. Due to the significant enhancement of the precipitation rate from the forced convection due to topographic influence (Milbrandt and Yau 2001), we use the observed rainfall over six weather stations from the Environment and Climate Change Canada (ECCC) report (ECCC 1997): Apica, Lac-Ha! Ha!, Rivière-Aux-Écorces, Bagotville A, Cap-Éternité, and Portage-Des-Roches. A table with the latitude, longitude, elevation (if available), and World Meteorological Organization (WMO) and/or ECCC numeric station identifier (ID) (if available) for each location is provided in Table 1. For all stations (see their locations in Figs. 2b,c), daily precipitation data are used for comparison with model and reanalysis values.

2) CRCM6/GEM5.1.1 CONFIGURATION AND EXPERIMENTAL SETUP

(i) CRCM6 configuration

The GEM5 model (McTaggart-Cowan et al. 2019), originally developed at ECCC, has been further adapted into the CRCM6/GEM5 developed within the Centre pour l'étude et la simulation du climat à l'échelle régionale (ESCER) center at Université du Québec à Montréal (UQAM). For lateral and surface boundary conditions needed in the CRCM6/GEM5 simulations, we use the ERA5 data from the European Centre for Medium-Range Weather Forecasts (ECMWF), which provides hourly atmospheric and oceanic surface conditions, at a spatial resolution of 31 km (Hersbach et al. 2020).

In our study, the considered configurations of the model with two resolutions are 12 km (horizontal grid spacing of 0.11°) and 2.5 km (horizontal grid spacing of 0.0225°), each of which includes 71 vertical levels. The 12-km resolution configuration employs the Kain–Fritsch deep convective (KFC) scheme (Kain and Fritsch 1990) alongside a shallow convection scheme (Bechtold et al. 2001). Moreover, the 2.5-km resolution is set up with and without the KFC deep convection parameterization in combination with the Kuo shallow transient scheme (Bélair et al. 2005). The 2.5-km model configuration, through the Kuo transient shallow convection scheme, allows for the parameterized condensation of water vapor, leading to precipitation. All simulations incorporate the Canadian Land Surface Scheme, version 3.6 (CLASS v3.6) (Verseghy 1991, 2000), which plays a significant role in simulating the interactions between the land surface and the atmosphere. The inclusion of this CLASS model in the CRCM6/GEM5, needed for long-term simulations, has improved the runoff and water characteristics of the soil compared to the Interaction Soil Biosphere Atmosphere (ISBA) scheme (Noilhan and Planton 1989; Noilhan and Mahfouf 1996; Bélair et al. 2003b,a) used in the GEM5.1.1 forecast model of ECCC, leading to more realistic occurrence and severity of the recent observed flood event in 2019 over the Ottawa River basin (see Benoit et al. 2022). For a comprehensive overview of the CRCM6/GEM5 model configuration, the reader is referred to Roberge et al. (2024).

(ii) Experimental setups

Utilizing the aforementioned model configuration, we conducted 10 distinct simulations, as shown in Table 2. Among these, two simulations employed a large 12-km resolution domain covering the Coordinated Regional Climate Downscaling Experiment (CORDEX) North American domain (shown in Fig. 2a), while eight simulations utilized the finer 2.5-km resolution, domain encompassing a significant portion of northeastern North America, specifically centered over southern Quebec (shown in the red box in Fig. 2a). The 2.5-km resolution simulation will allow to evaluate some potential added values in the characteristics of this storm and precipitation patterns in the region. Additionally, we are using the same resolution and nearly identical settings as the ECCC's High Resolution

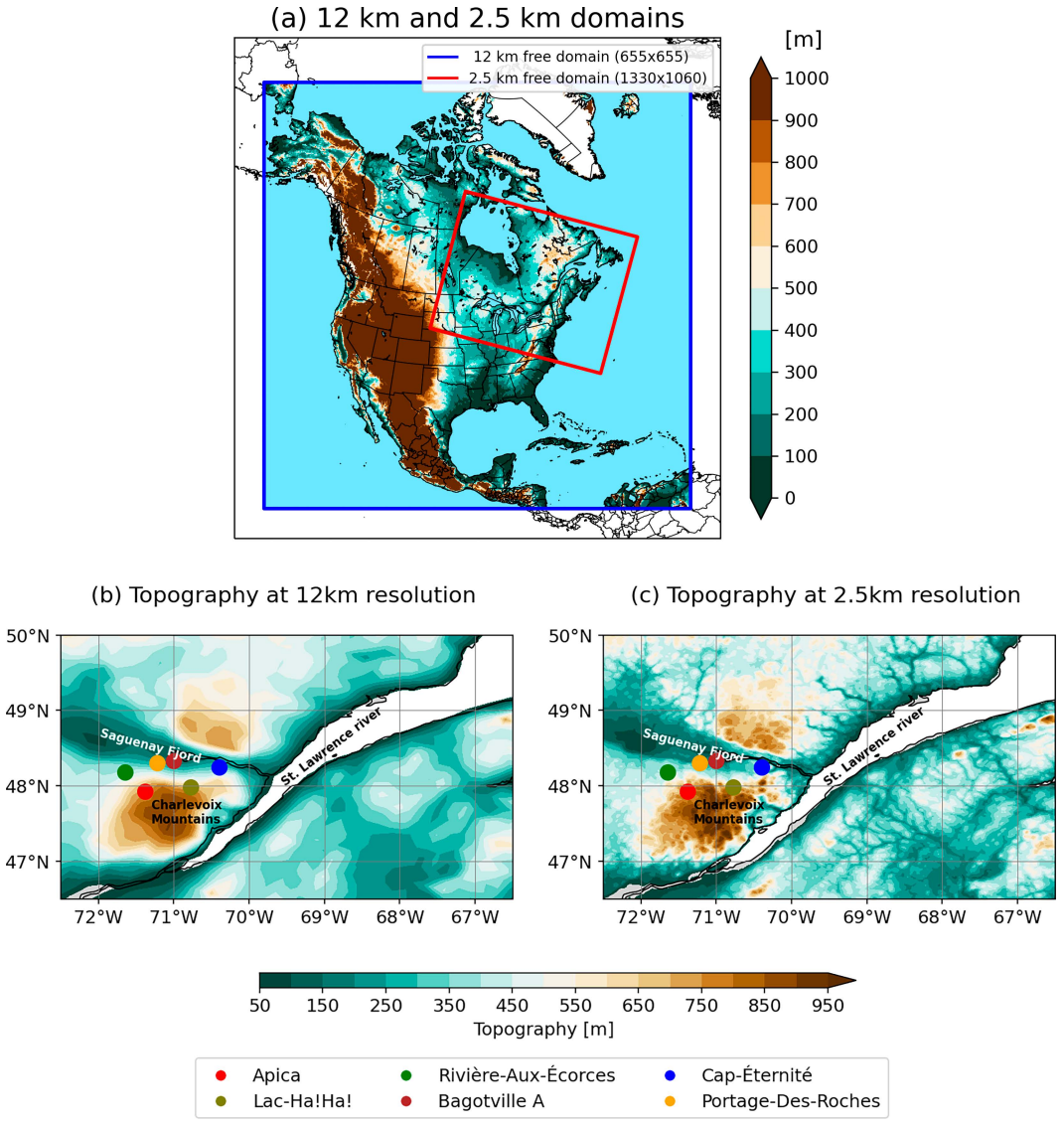

FIG. 2. The model domain and topography utilized in the 12- and 2.5-km simulations conducted with CRCM6/GEM5: (a) The North American domain for the 12-km simulation is marked with a blue box, and the smaller domain at 2.5-km covering Quebec Province and its surrounding regions is highlighted in red; (b) the topography of the study region at 12-km resolution; and (c) the topography of the study region at 2.5-km resolution. The points indicate the weather stations distributed across the plain, foothills, and high-altitude areas that are used to evaluate the CRCM6/GEM5 simulations over the study area.

Deterministic Prediction System (HRDPS), which has been well adjusted and extensively validated by ECCC for operational forecasts. The model is initialized 1 day prior to the extreme event, specifically on 18 July 1996, and extended up to 1 day following the event, ending on 21 July 1996. The experimental design encompassed various combinations, including large-scale SN, convection parameterization, and surface moisture considerations, as discussed in Table 2.

(iii) Domain of simulation

The model configuration is tailored to the study requirements and encompasses two domain sizes. The larger domain, with a resolution of 12 km, covers the CORDEX North American domain (Giorgi and Gutowski 2015), as delineated by the blue line in Fig. 2a, spanning dimensions of 655 × 655 grid points (including the sponge zone). The domain of the finer resolution of 2.5 km covers only northeastern North America, centered over southern Quebec. This smaller domain, represented by the red box in Fig. 2a, includes 1330 × 1060 grid points (including the sponge zone).

Topography with mountains between 900 and 1200 m in the Laurentian and Valin Mountains (see Fig. 2b) plays a crucial role over the study region during precipitation events, as it influences the occurrence, amount, and duration of precipitation. Its

TABLE 2. Experimental setups in the CRCM6/GEM5 model for the current study using different resolutions and configurations. All simulations use atmospheric and oceanic boundary conditions from the ERA5 reanalysis. As mentioned in the text, the ISMC varies from ERA5-Land and CRCM6-UAA in the identified simulations at 2.5 km. The KFC scheme is applied (indicated by a "Yes" for deep convection parameterization) where indicated. CRCM6-UAA represents land surface moisture from a 12-km long-term simulation from the same model. All simulations are initialized on 18 Jul 1996 and end on 21 Jul 1996.

Resolution (km)	Initiation date	End date	Spectral nudging	Parameterization (deep convection)	Initialized soil moisture	Experiments
12	18 Jul	21 Jul	No	Yes	ERA5-Land	Experiment I
	18 Jul	21 Jul	Yes	Yes	ERA5-Land	Experiment II
2.5	18 Jul	21 Jul	No	Yes	ERA5-Land	Experiment III
	18 Jul	21 Jul	No	Yes	CRCM6-UAA	Experiment IV
	18 Jul	21 Jul	No	No	ERA5-Land	Experiment V
	18 Jul	21 Jul	No	No	CRCM6-UAA	Experiment VI
	18 Jul	21 Jul	Yes	Yes	ERA5-Land	Experiment VII
	18 Jul	21 Jul	Yes	Yes	CRCM6-UAA	Experiment VIII
	18 Jul	21 Jul	Yes	No	ERA5-Land	Experiment IX
	18 Jul	21 Jul	Yes	No	CRCM6-UAA	Experiment X

hydrographic basin drains the major tributaries located in the central part of Québec and extends over around 700 km from the Peribonka watershed toward the Saint Lawrence River. The region's elevation ranges significantly, within the estuary of the Saint Lawrence River (hereafter called bay), and Saguenay Fjord, are the Laurentian Mountains (especially Charlevoix Mountains) to the south of the Saguenay Fjord (hereafter called highlands), while these valleys and fjords (hereafter called lowlands) are close to sea level. The study area, spanning from 46.5° to 50°N and from 66.5° to 72.5°W, is indicated in Figs. 2b and 1c with the terrain elevations reaching 1100 m at a resolution of 2.5 km (see Fig. 2c). In fact, at a finer resolution of 2.5 km (see Fig. 2c), detailed topographic information provides potentially higher effects in modeling forced convective activity. The weather stations from ECCC (Table 1), shown in colored scatter points in Figs. 2b and 2c, are used to evaluate the simulated precipitation over the study area.

(iv) Modeling deep convection

Deep convection can be represented in atmospheric models either through parameterization schemes like KFC or by explicitly resolving deep convective processes in high-resolution simulations. The KFC scheme simulates deep convection by triggering convective events based on parcel buoyancy and lifting from low-level convergence (Kain and Fritsch 1990). It parameterizes entrainment and detrainment processes to represent the vertical transport of heat and moisture. The scheme adjusts atmospheric stability by redistributing mass and energy, thus influencing the intensity and timing of precipitation. In CP simulations, deep convection is explicitly resolved by the model without relying on parameterization schemes like KFC. The model captures the development of convective cells based on thermodynamic and dynamic conditions (e.g., buoyancy, wind shear, and heat and moisture transports) at fine spatial and temporal scales. This not only allows for more realistic representation of convective structure, timing, and intensity but also increases sensitivity to model resolution and surface conditions (e.g., Prein et al. 2017; Kendon et al. 2021).

(v) SN

SN is a technique used in RCM simulation to incorporate large-scale forcing and reduce the internal variability of RCMs by nudging large-scale atmospheric features (see Biner et al. 2000; Alexandru et al. 2009; Separovic et al. 2012). This method essentially "nudges" an RCM toward the behavior of a driving simulation or reanalysis product, helping to maintain coherence with broader spatial patterns between the driving fields and the simulated ones within the domain of the RCM. The SN is done using large-scale atmospheric features (i.e., wind fields) by applying a correction based on the difference between the regional model's large-scale components and those from a global climate model (GCM) or reanalysis data (von Storch et al. 2000; Miguez-Macho et al. 2004). At the same time, the atmospheric variables in the RCM are decomposed into their spectral components using a Fourier transform (Miguez-Macho et al. 2005). The large-scale components (planetary wavelength) are then compatible with the corresponding components from the GCM or reanalysis data (Bowden et al. 2012). The nudging term adds to the RCM equations and is proportional to the difference between the regional model's large-scale components and those from the large-scale driving conditions (Alexandru et al. 2009). The strength of the nudging term can be tuned to balance between maintaining large-scale coherence and allowing the regional model to develop its own small-scale features (von Storch et al. 2000).

To optimize our model's performance in simulating this case study of precipitation extremes and capturing regional-scale details influenced by large-scale atmospheric conditions, we employ SN to both the 12- and 2.5-km simulations, specifically targeting the horizontal wind components. For the 12-km resolution, we adopt the SN settings described in Roberge et al. (2024). However, for the 2.5-km resolution, we make modifications to enhance the strength of the SN. We employ five aspects that control the strength of the SN. These aspects are applied sequentially and include the filter in spectral space (horizontal), the shape of the vertical profile, the intensity of nudging applied at each time step, the nudging interval, and the nudging weight. It is crucial to adjust the nudging strength

according to the wavelength. The filter in spectral space, which depends on the resolution, is set to 200 km for the small scale and 900 km for the large scale. To control the vertical profile, the nudging for the lower level starts at hybrid level 0.7 (which is approximately 700 hPa) and gradually increases until 0 (the top of the model) following a cosine-squared function (Schubert-Frisius et al. 2017). The SN is applied at each time step, with a relaxation time scale of 8 h. The nudging interval is set to 60 s, and the nudging weight in the temporal space is disabled.

The selection of this small-scale cutoff value in spectral nudging depends directly on the resolution of the driving data. In our simulations, the cutoff wavelength was set to approximately 6 times the horizontal resolution of the forcing dataset. For example, when using a driving dataset with a horizontal resolution of approximately 30 km, the cutoff is typically set to around 200 km. This ensures that only the large-scale synoptic features with wavelengths exceeding 200 km are constrained toward the driving data, while the smaller mesoscale and local features, such as convective storms, localized winds, and topographically influenced flows, are left free to develop naturally within the nested model domain through its own high-resolution dynamics and physical parameterizations. Nudging these scales means the model continuously adjusts both the amplitude and phase of these large-scale waves to stay consistent with the driving data, such as ERA5 reanalysis.

Spectral nudging is applied more strongly at 2.5-km resolution because high-resolution models can resolve finer-scale atmospheric features that are more sensitive to internal variability and may diverge significantly from the driving large-scale fields. Stronger nudging helps to constrain these small-scale developments and maintain consistency with the large-scale atmospheric state, which is especially important when evaluating the influence of boundary conditions. In contrast, at the coarser 12-km resolution, the model inherently represents larger-scale processes and exhibits less internal variability, so a weaker nudging strength is sufficient to guide the simulation without overly constraining it.

(vi) Soil moisture initializations

Soil moisture plays a crucial role in the development of extreme weather events, influencing the intensity and duration of precipitation (Taylor et al. 2012), mainly through the recycling of precipitation through surface evaporation (see Schaefli et al. 2012). Initial soil moisture conditions (ISMCs) can significantly affect the model's ability to accurately simulate extreme rainfall events. To assess the sensitivity of the model configuration to ISMCs, we designed a simple experiment (using two different soil moisture setups) to evaluate whether variations in soil moisture influence simulated precipitation. The goal is to determine if the model can be effectively used in an "event mode" experimental setting (approximately 8 days). In this mode, the model is expected to simulate short-term meteorological events, such as storms, even when the initial conditions are not fully compatible with the higher-resolution domain (e.g., using 2.5-km resolution initialized from a 12-km simulation). By perturbing the initial soil moisture values across the domain, we aim to understand the sensitivity of the model to different surface conditions. The results will help inform better strategies for initializing the model. In the first setup, ISMCs (Table 3) from ERA5-Land are used. In the second, ISMC is incorporated from a preexisting CRCM6/GEM5 long-term simulation at 12-km resolution (hereafter, CRCM6-UAA simulation). For this setup, sea surface temperature and sea ice concentration are incorporated from ERA5 reanalysis data, and the variables from Table 3 have been incorporated from the CRCM6-UAA. The CRCM6-UAA simulation is initialized on 1 January 1979 using the atmospheric conditions from ERA5, and land initial conditions are from the previous CORDEX-North America simulation using the precedent version of our RCM, i.e., the CRCM5 (Zadra et al. 2008). The soil volumetric water content for both setups is shown in Fig. 3, with data from ERA5-Land presented in Fig. 3a, the CRCM6-UAA simulation depicted in Fig. 3b, and the percentage changes shown in Fig. 3c. In general, the CRCM6-UAA simulation contains drier surface conditions than the soil moisture conditions from ERA5-Land. However, the limitation of the current modeling framework lies in its restricted capability to test a wide range of ISMCs when the CLASS land surface scheme is used.

TABLE 3. Environmental variables and units.

Variable	Unit
Surface temperature	K
Soil temperature	K
Soil volumetric water content	$m^3\ m^{-3}$
Soil volumetric ice content	$m^3\ m^{-3}$
Snow water equivalent (SWE)	$kg\ m^{-2}$
Albedo of snow	Fraction
Sea ice temperature	K
Sea ice thickness	m
Glacier temperature	K
Snow depth	cm
Snow density	$kg\ m^{-3}$
Canopy temperature	K
Ground snow temperature	K
Temperature of water lying on surface	K
Water retained on vegetation	$kg\ m^{-2}$
Height of water lying on surface	m
Water in the snowpack	$kg\ m^{-2}$
Snow stored on canopy	$kg\ m^{-2}$
Canopy growth factor	Dimensionless
Temperature at the base of soil water column	K

c. Analysis methods and validation procedure

To evaluate the model's performance in simulating extreme rainfall events (e.g., Llerena et al. 2023), we compared the first daily accumulated rainfall data from all simulations presented in Table 2 with the ones from gridded reanalysis datasets of ERA5-Land and RDRS. For a consistent comparison, all gridded datasets are interpolated to the same 2.5-km resolution of the CRCM6/GEM5 model. The comparison focuses on the spatial distribution of daily precipitation and includes also the observed rainfall data from six weather stations presented in Figs. 2b and 2c.

The storm track is simply followed by identifying the minimum MSLP value on an hourly basis over ERA5 and the

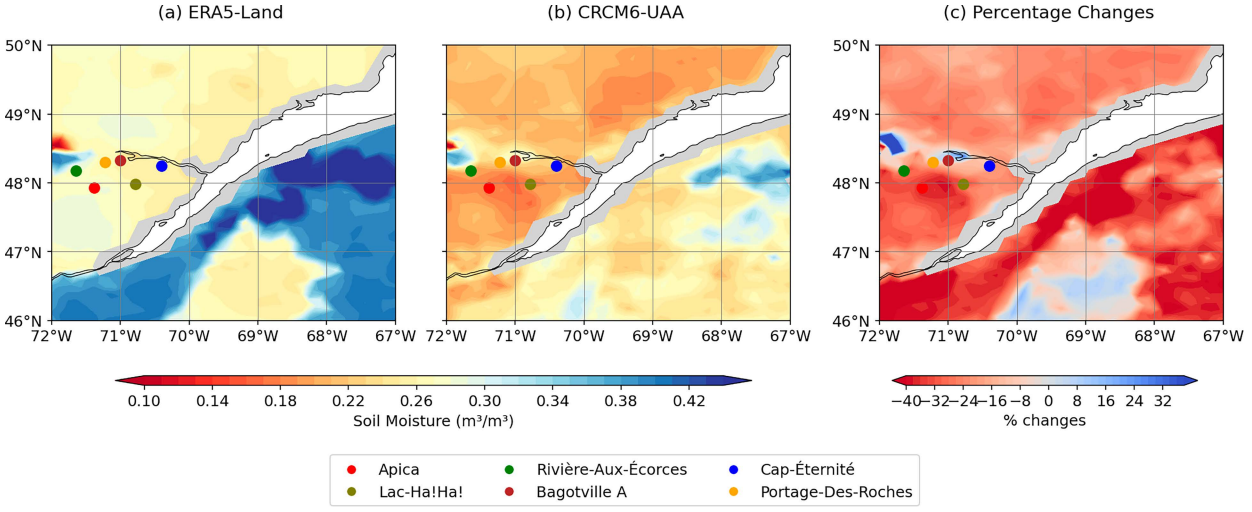

FIG. 3. Soil moisture from (a) the ERA5-Land dataset and (b) the CRCM6-UAA simulation on 18 Jul 1996, which are used to initialize the CRCM6/GEM5 simulation at 2.5 km. (c) The percentage difference in CRCM6-UAA over ERA5-Land. The CRCM6-UAA simulation reflects ISMC derived from a 12-km long-term simulation, while both datasets are applied to downscale the simulation at 2.5-km simulation grid.

2.5-km domain grid, spanning from 1200 UTC 19 July to 0000 UTC 22 July. The latent heat flux (LHF) is diagnosed to quantify the energy transferred by moisture exchange between the surface and atmosphere, driving weather systems and the hydrological cycle (Holton and Hakim 2013), and is calculated using

$$\mathrm{LHF} = -\frac{L_v \omega q}{g}. \tag{1}$$

Further, the moisture flux vector at a given pressure level is calculated from

$$\mathbf{F}_q = q\cdot\mathbf{V} = q\cdot(u, v), \tag{2}$$

where the total moisture flux $\mathbf{Q}$ across all pressure levels is

$$\mathbf{Q} = \int_{p_{\mathrm{top}}}^{p_s} \mathbf{F}_q \frac{dp}{g} = \int_{p_{\mathrm{top}}}^{p_s} q\cdot\mathbf{V}\frac{dp}{g}.$$

To move on to VIMD,

$$\mathrm{VIMD} = \int_{p_{\mathrm{top}}}^{p_s} \nabla\cdot\mathbf{Q}\frac{dp}{g}, \tag{3}$$

where $L_v = 2.5\ \mathrm{J} \times 106\ \mathrm{J\ kg^{-1}\ J\ kg^{-1}}$ is the latent heat of vaporization, $g = 9.81\ \mathrm{m\ s^{-2}}$ is the gravitational acceleration, ω is the vertical velocity in pressure coordinates, q is the specific humidity, u and v are the zonal and meridional wind components, $\mathbf{F}_q$ is the horizontal moisture flux vector, and p_s and p_{top} are the pressure at surface and upper level (100 hPa), respectively.

To evaluate the performance of all simulations at the hourly scale, all simulated and reanalysis datasets are compared at gridpoint values close to each station through a boxplot that includes the median, interquartile range, and outliers, using a 95% confidence interval. Also, to compare the continuous probability distribution and shape of all datasets, we use the kernel density estimate (KDE) approach, also at a 95% confidence level, across the six weather stations. The evaluation is performed over 2 consecutive days (19 and 20 July 1996) to assess the model's ability to replicate extreme rainfall events over the duration of the storm. The day measurement period spans from 0900 UTC to the following day at 0800 UTC, in accordance with the reporting standards of the ECCC report (ECCC 1997), and all times are referenced in coordinated universal time (UTC).

3. Results

a. Daily observed rainfall versus reanalysis datasets

The daily rainfall spatial pattern from observed and reanalysis rainfall data across various stations over the Saguenay region is depicted in Table 4. As shown from the observed rainfall at the weather stations in Apica, Lac-Ha! Ha!, Rivière-Aux-Écorces, Bagotville A, Cap-Éternité, and Portage-des-Roches recorded

TABLE 4. Daily observed and gridded rainfall (mm day^{-1}) data from ERA5-Land and RDRS products across various stations over the Saguenay region for 19 and 20 Jul 1996. The Environment Canada Report (ECR) data sourced from the ECCC report (ECCC 1997).

	ECR		ERA5-Land		RDRS	
Station	19 Jul	20 Jul	19 Jul	20 Jul	19 Jul	20 Jul
Apica	162.5	104.1	94.32	65.87	110.06	30.04
Lac-Ha! Ha!	157.7	88.6	101.79	76.66	83.56	42.36
Rivière-Aux-Écorces	147.3	127.0	86.17	73.40	98.39	68.49
Bagotville A	128.6	35.5	99.92	64.60	98.21	63.82
Cap-Éternité	151.3	6.0	95.14	45.86	81.60	32.36
Portage-Des-Roches	144.7	63.5	98.63	71.75	104.17	79.82

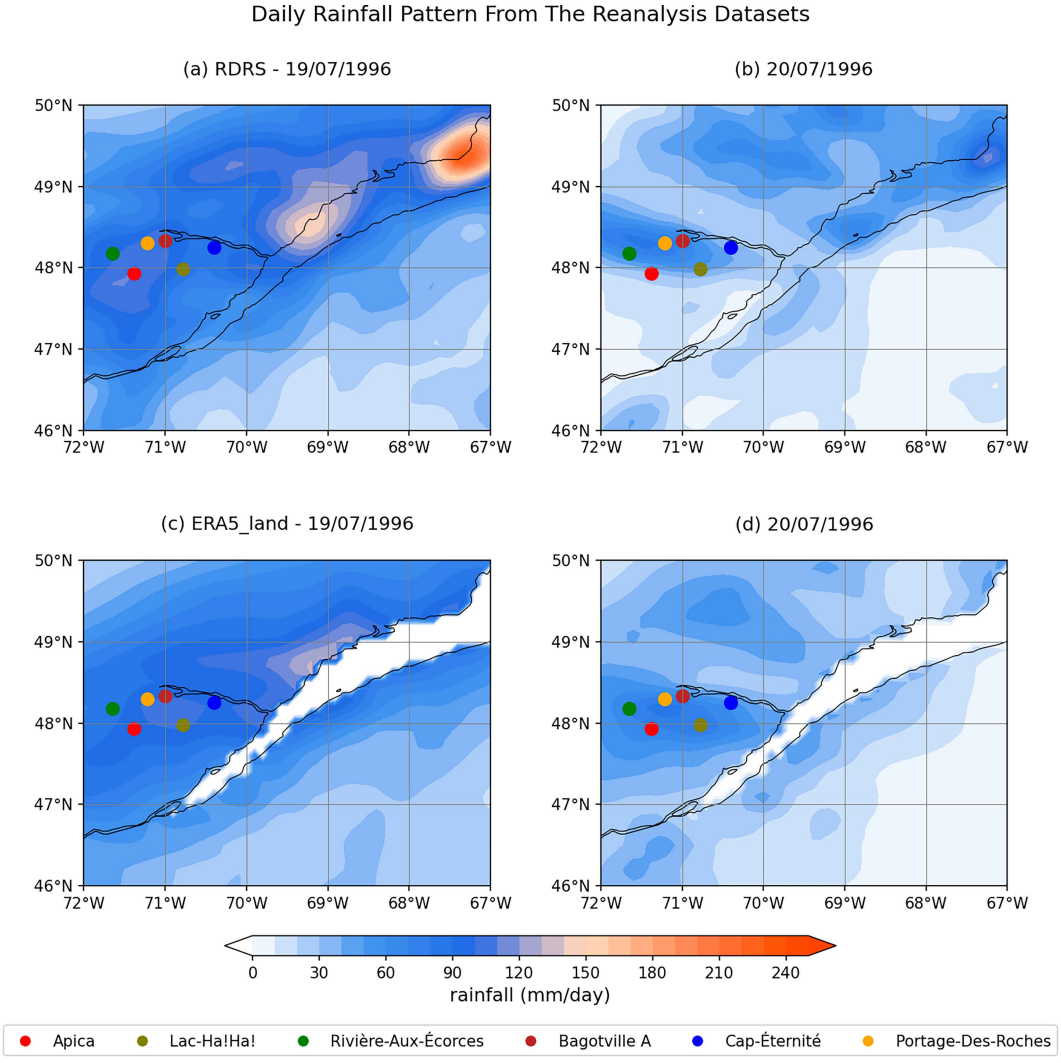

FIG. 4. Spatial distribution of rainfall in Saguenay for the 2 consecutive days (a)–(c) 19 and (b)–(d) 20 Jul. (a),(b) Gridded rainfall data from RDRS and (c),(d) gridded rainfall data from ERA5-Land. Each panel includes weather stations of ECCC. The time period is measured from 0900 UTC to the following day at 0800 UTC.

totals were 162.5, 157.7, 147.3, 128.6, 151.3, and 144.7 mm, respectively, on 19 July. On 20 July, the respective amounts were less important varying from 104.1, 88.6, 127, 35.5, 6, and 63.5 mm. In contrast, the values from the ERA5-Land and RDRS datasets show systematically lower amounts across the region. For ERA5-Land, the totals are 94.32/65.87, 101.79/76.66, 86.17/73.4, 99.92/64.6, 95.14/45.86, and 98.63/71.75 mm on 19/20 July, respectively, for each station. Similarly, the RDRS dataset shows 110.06/30.04, 83.56/42.36, 98.39/68.49, 98.21/63.82, 81.6/32.36, and 104.17/79.82 mm on 19/20 July. Therefore, the rainfall from the gridded datasets (ERA5-Land and RDRS) shows almost half that compared to the cumulative (2-day) rainfall measured at the weather stations, suggesting a systematic underestimation of intensity and duration of daily reanalysis values with respect to observed point or local-scale precipitation data.

The daily spatial rainfall pattern over the region for 19 and 20 July is depicted in Fig. 4. The gridded data from RDRS and ERA5-Land show significant variability in rainfall amount across the region, with both datasets indicating a pronounced rainfall pattern on the first and second days of the extreme event. An average daily rainfall of 96 mm is recorded in both datasets across the six weather stations on the first day of the extreme event, i.e., 19 July (Table 4). The ERA5-Land and RDRS gridded datasets showed daily average rainfall amounts of 66.39 and 52 mm, respectively, over the same six stations (Table 4).

b. Daily rainfall pattern as simulated at 12-km resolution

Figure 5 illustrates the spatial distribution of extreme rainfall over the Saguenay region, simulated by the CRCM6 at a 12-km resolution for 2 consecutive days. The simulation without SN clearly enhanced simulated rainfall intensity and its gradient compared to the reanalysis data (from both RDRS and ERA5-Land; see Fig. 4), with higher rainfall values found

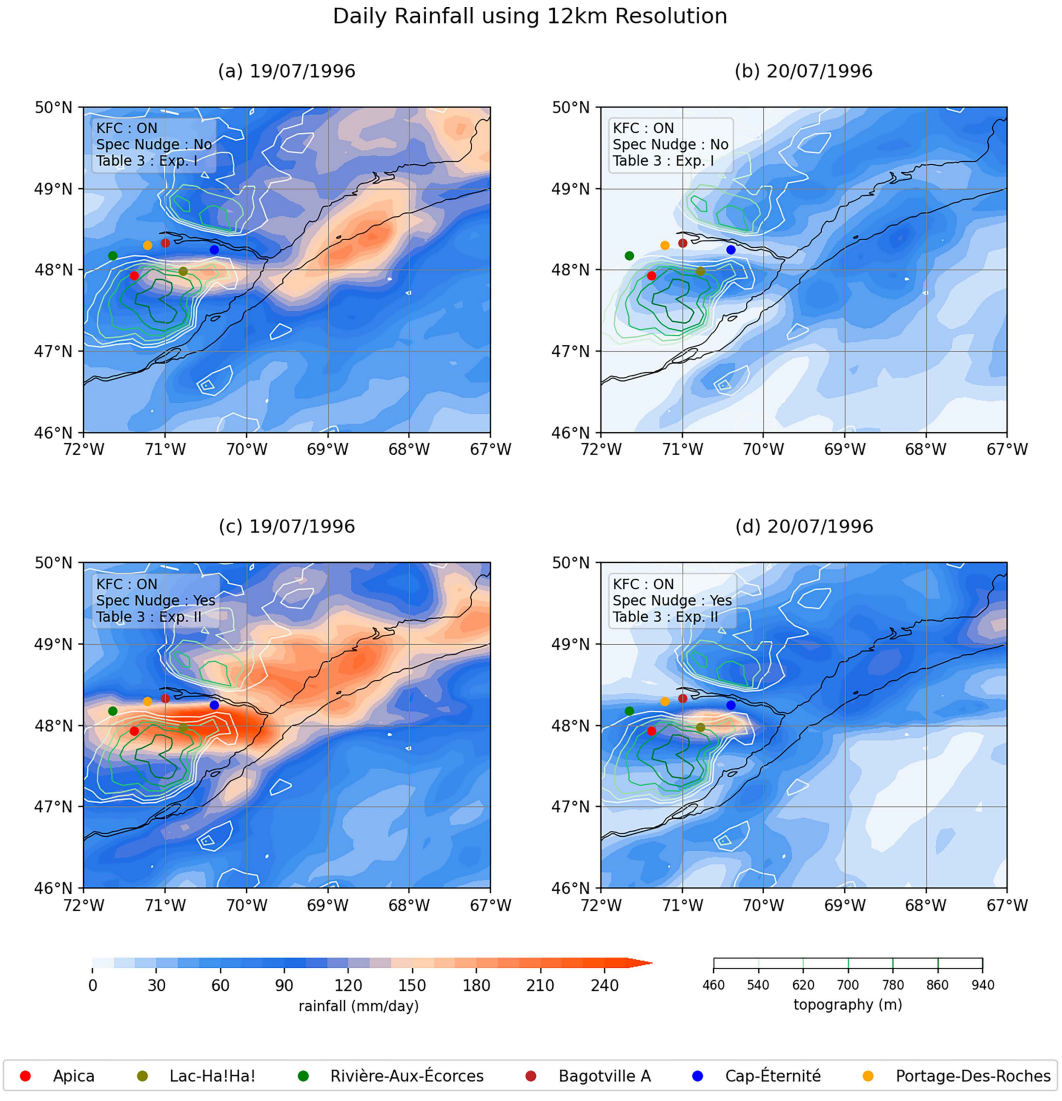

FIG. 5. Spatial distribution of extreme rainfall simulated by the model at a 12-km resolution over the Saguenay region for consecutive days. (a),(b) The rainfall distribution using the 12-km resolution model without SN (refer to Table 2; experiment I) for 19 and 20 Jul, and (c),(d) the same applying SN (refer to Table 2; experiment II) for the same dates. Each panel includes weather stations covering the flooded region.

in the highlands and foothills. On 19 July, rainfall in the highland regions reaches mostly less than 100 mm, dropping to approximately 30 mm on 20 July. In addition, simulations with SN exhibit a better agreement with the weather station values, capturing some aspects of the spatial distribution of extreme rainfall indicated with RDRS and ERA5-Land. Notably, the grid point close to the location of the weather stations shows insufficient rainfall on 19 July, as seen in Fig. 5a. A significant increase is observed with SN, showing more than 120 mm of rainfall over the highland region, with the mountain peak receiving over 150 mm of rainfall, as shown in Fig. 5c. Similarly, areas with less than 40 mm of rainfall on 20 July in Fig. 5b show substantial increases and a larger rainfall band over the mountains with SN in Fig. 5d.

c. *Added value from CPM and sensitivity from soil moisture*

This section examines the added value derived from a CPM and explores the sensitivity to ISMC. Figures 6a–f illustrate daily rainfall distribution at a 2.5-km resolution (Figs. 6a–c) utilizing the KFC deep convection scheme and (Figs. 6d–f) deep convection deactivated for 19 July 1996. The simulations using the ERA5-Land ISMCs reveal rainfall amounts below 100 mm over most weather stations (Fig. 6a), with a deep rainband over the south of bay and highland regions. Moreover, rainfall significantly increases with a deep rainband exceeding 110 mm over the highland region and the bay when incorporating ISMC from the CRCM6-UAA simulation (Fig. 6b). Heavy rainfall

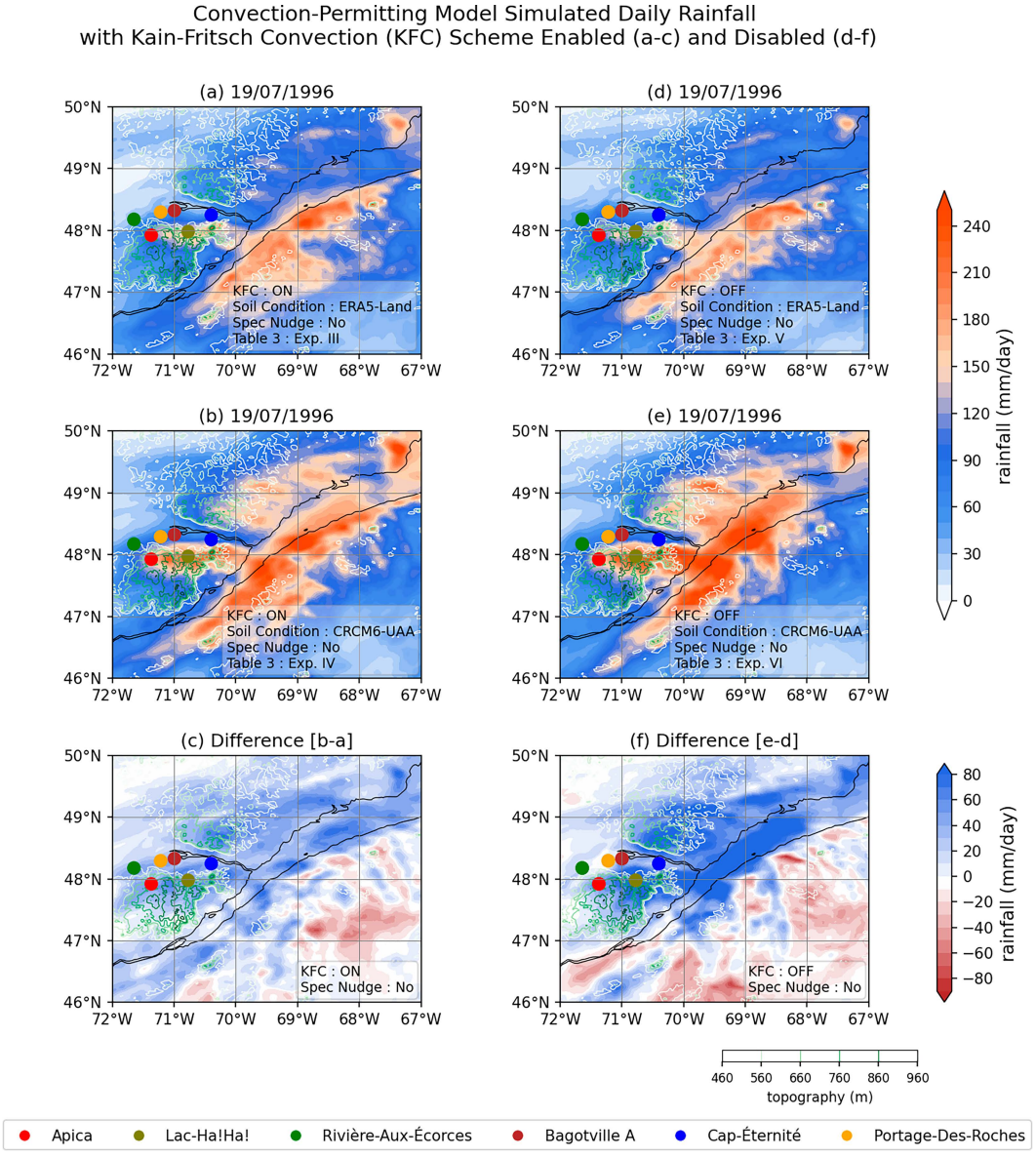

FIG. 6. Daily rainfall distribution in the 2.5-km resolution using the KFC scheme (a)–(c) activated and (d)–(f) deactivated. (a),(d) Rainfall distribution with land initial condition from ERA5-Land and atmospheric initial condition from ERA5 (refer to Table 2; experiments III and V) for 19 Jul, and (b),(e) the same initial and lateral boundary atmospheric conditions from ERA5 and ISMC from CRCM6-UAA 12-km simulation from the same model (refer to Table 2; experiments IV and VI) for the same date. (c)The difference between (b) and (a); (f) the difference between (e) and (d). The CRCM6-UAA simulation integrates ISMC derived from a 12-km long-term simulation to downscale the simulation to a 2.5-km grid. Each panel includes weather stations covering the flooded region.

patterns also emerge over the northern part and the bay. The differences between the second and first panels of each column underscore the added value in improving extreme precipitation patterns, with enhanced rainfall over the northern bay and highland regions more pronounced when CRCM6-UAA ISMC is used (Fig. 6c). This demonstrates the CRCM6 sensitivity to ISMC in refining extreme event simulation (e.g., Ferrett et al. 2021).

Using the CRCM6 with deep convection deactivated (Figs. 6d–f), rainfall is distributed nearly uniformly over the northern bay and adjacent station regions, reaching approximately 80 mm on the first day (Fig. 6d). A narrow rainband, akin to Fig. 6a, is evident over the southern bay and highland regions. Moreover, incorporating ISMCs from the CRCM6-UAA simulation results in a significant increase in rainfall, with an intensified rainband exceeding 150 mm over the highland region and the bay (Fig. 6e). Intensified rainfall over the northern bay and highland regions is more evident of the extreme event when CRCM6-UAA ISMC is used

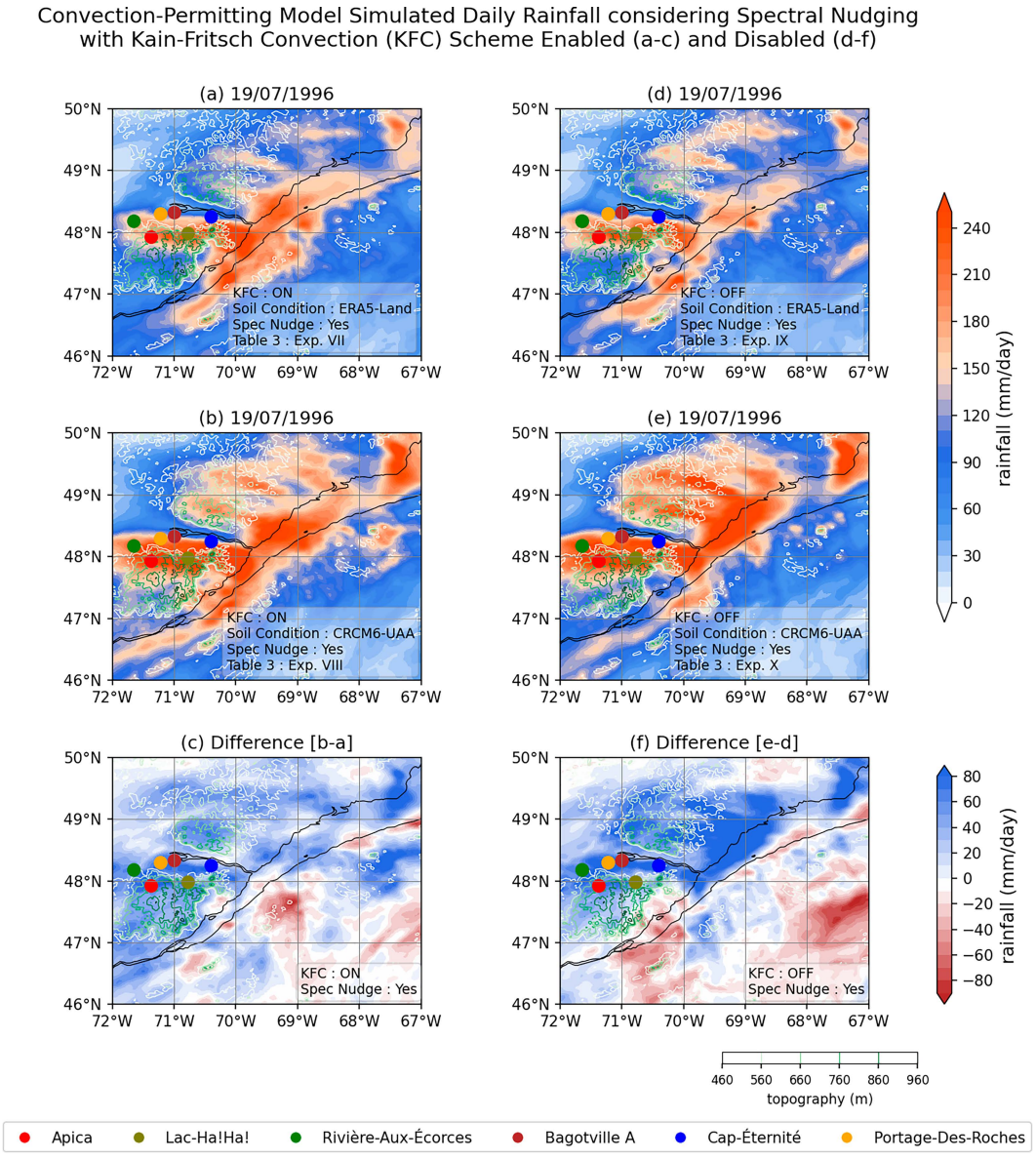

FIG. 7. As in Fig. 6, but with the SN, as described in Table 2 (experiments VII–VIII and IX–X).

(Fig. 6f), showing a significant positive anomaly of over 70 mm in the northern bay on the day near the stations. This highlights the CRCM6 sensitivity to ISMC in the CP configuration.

d. Importance of SN for precipitation extremes

Figures 7a–f illustrate the daily rainfall distribution at a 2.5-km resolution (Figs. 7a–c) using the KFC scheme and (Figs. 7d–f) deactivated KFC with SN applied. This figure replicates Fig. 6 but includes SN. Figure 7a reveals rainfall amounts around 100 mm over most weather-station-located regions, with mountains receiving over 100 mm. The deep rainband seen in Figs. 6a and 6b over the southern bay propagates northward. When ISMC from the CRCM6-UAA simulation is incorporated, the rainfall amount is significantly increased. At the same time, the distribution pattern improves with a deep rainband exceeding 130 mm over the highland region and the bay on the first day (Fig. 7b). Heavy rainfall patterns also emerge over the northern bay and highland regions. The differences between the second and first panels of each column highlight the added value from the deep convection parameterization in enhancing the spatial pattern of the climate extreme simulation when CRCM6-UAA ISMC is applied (Fig. 7c).

Figures 7d–f extend the findings of Figs. 6d–f by applying SN. Using the CPM setup in Fig. 7d, we observe an enhanced rainfall distribution over the northern bay and highland regions compared to Figs. 7a–c. Notably, there is a marked reduction in rainfall over the bay and the southern part of the bay in Fig. 7d compared to Fig. 7a. Using the SN setup, the highland region receives approximately 130 mm of rainfall on 19 July. Moreover, the rainfall over the northern part of the bay becomes

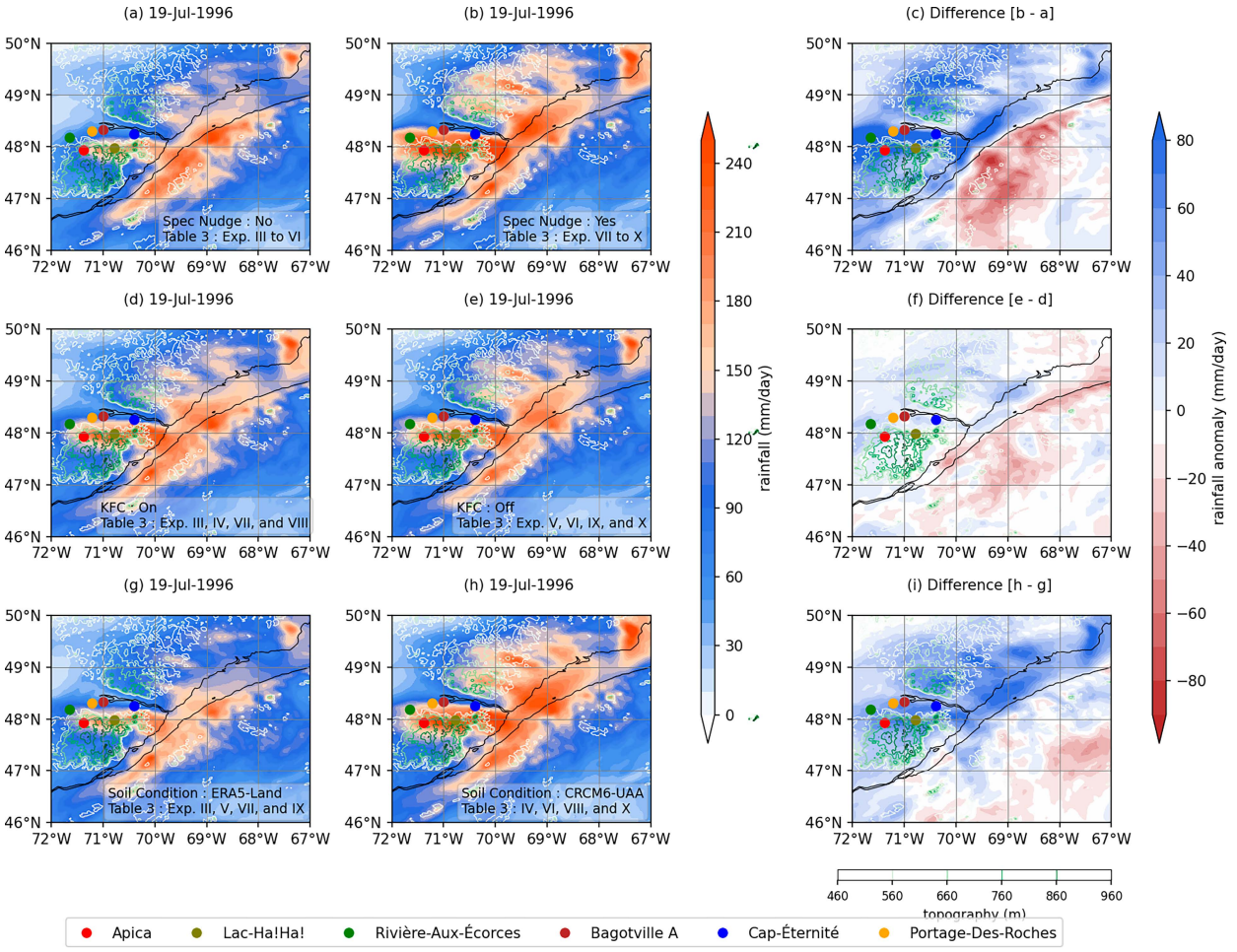

FIG. 8. Sensitivity of the 2.5-km climate model in simulating extreme rainfall event by considering different simulations with SN (on/off), deep convection (on/off), and the ISMC (ERA5-Land/CRCM6-UAA). (a),(b) The sensitivity in rainfall distribution using without (applying experiments III–VI from Table 2) and with (considering experiments VII–X from Table 2) SN and (c) the difference between (b) and (a); (d),(e) the sensitivity considering the deep convection on (considering experiments III, IV, VII, and VIII from Table 2) and off (considering experiments V, VI, IX, and X from Table 2) and (f) the difference between (e) and (d). (g),(h) The sensitivity considering ISMC from ERA5-Land (considering experiments III, V, VII, and IX from Table 2) and from the CRCM6-UAA simulation (considering experiments IV, VI, VIII, and X from Table 2), and (i) the difference between (h) and (g).

more pronounced and intense during extreme weather events, as shown in Fig. 7e. This intense rainfall pattern is also associated with higher rainfall amounts (greater than 130 mm) compared to the simulations with deep convection turned on, as shown in Fig. 7b. The improvement in model simulations using ISMC from the CRCM6-UAA simulation for the same dates is clearly evident in Fig. 7f, and the dynamics are explained in section 4 and section 5.

A sensitivity analysis was conducted to evaluate the impact of SN, deep convection, and ISMC on the CRCM6 model's ability to simulate extreme rainfall events. Figure 8 illustrates the sensitivity of the CPM at a 2.5-km resolution for the first day of the extreme event, during which an excessive amount of rain was received on 19 July 1996. The sensitivity is assessed by comparing simulations with and without SN, deep convection turned on and off, and ISMC from ERA5-Land versus a CRCM6-UAA simulation. The analysis is based on the mean of groups of simulations from the same setup, highlighting the sensitivity. Figures 8a and 8b reveal that SN improves the model's ability to simulate extreme rainfall events. The rainfall intensity over the Saguenay region is particularly noticeable using the SN setup. A rainfall difference of more than 80 mm is depicted over the flooded region, while a reduction in rainfall is noted over the eastern part of the bay on 19 July 1996 (Fig. 8c). An interesting observation emerges from the sensitivity analysis of the deep convection scheme (Figs. 8d,e). The spatial distribution appears quite similar when the KFC scheme is turned on or off in the CPM. However, a rainfall variation of 10–20 mm can be observed over some regions (Fig. 8f). Finally, the sensitivity analysis highlights the critical role of accurate ISMC data in refining climate simulations (Figs. 8g,h), with the model showing a significantly enhanced rainfall distribution when the ISMC from the CRCM6-UAA simulation is used. The model appears

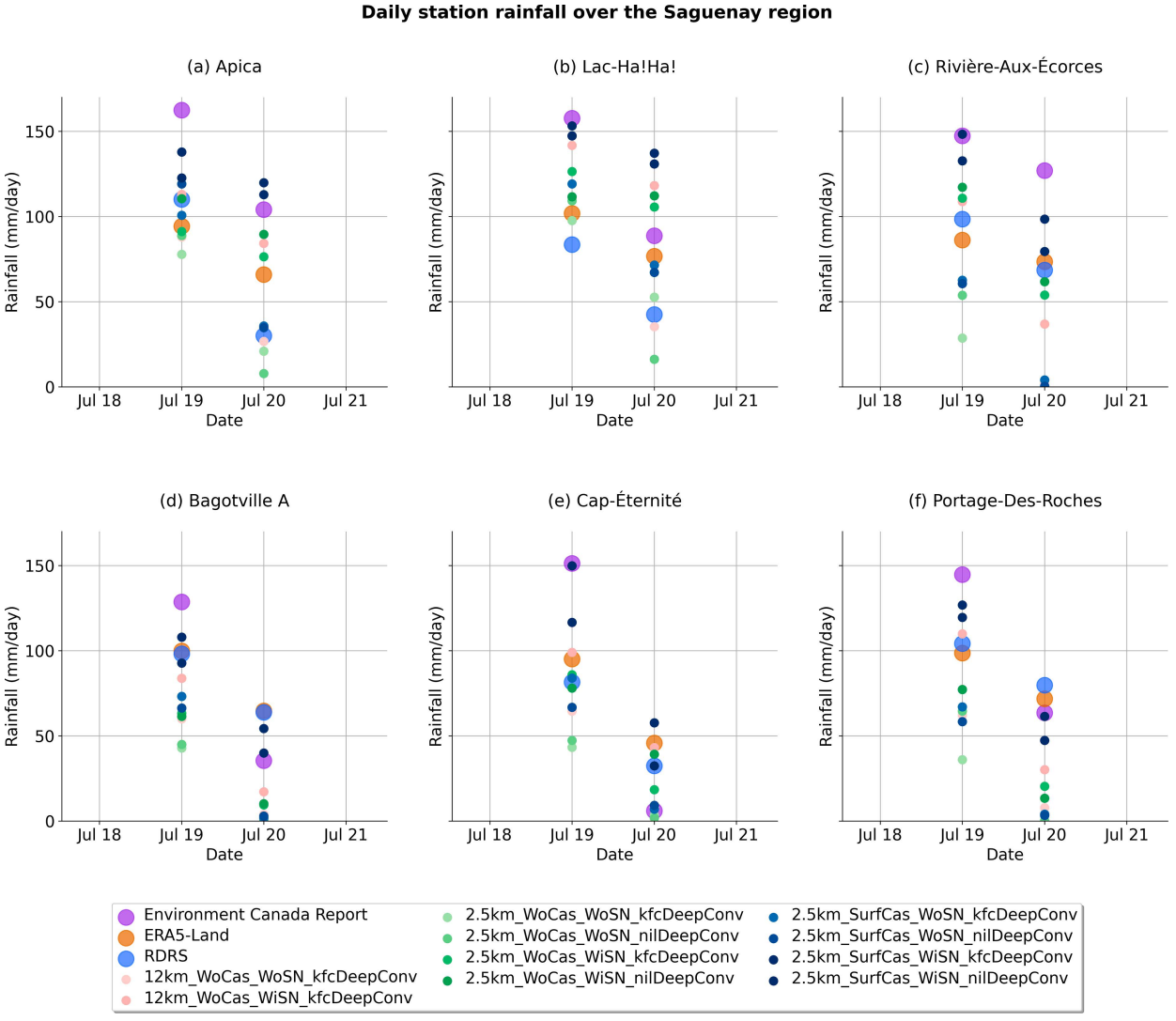

FIG. 9. (a)–(f) Daily rainfall measurements from six different stations during extreme precipitation events. The larger scatter points indicate daily rainfall from observed and reanalysis datasets, while smaller scatter points represent each dataset with a unique color, as detailed in Table 1 (experiment I–experiment X). Observed station rainfall data are sourced from the ECCC report (Table 1, ECCC 1997). In the legend, "WoCas" denotes ISMC from ERA5-Land, "SurfCas" represents ISMC from a 12-km CRCM6-UAA simulation derived from long-term simulation data, "WoSN" indicates simulations without SN, "WiSN" represents simulations with SN, "kfcDeepConv" signifies simulations using the KFC convection parameterization, and "nilDeepConv" represents simulations in which KFC remains deactivated.

very sensitive to ISMC, and an enhancement of more than 40 mm of rainfall is observed over Saguenay and its surrounding region (Fig. 8i). In contrast, simulations using ERA5-Land ISMC data significantly underestimate the rainfall distribution over the region.

e. Added value on daily rainfall measurements at stations near the flooded region

The added value in accumulating the daily rainfall with the different modeling setups is measured at the weather stations near the flooded region (Fig. 9), highlighted in Fig. 2. Larger scatter points indicate the data from observed and reanalysis datasets, while smaller scatter points represent each model simulated dataset with a unique color, as detailed in Table 2.

The daily rainfall measurements over the weather station show significant variability across different simulations by capturing the extreme precipitation events more accurately compared to the observations. The panels reveal a substantial underestimation in the ERA5-Land and RDRS gridded rainfall compared with observed station rainfall, also previously noted in section a in Table 4. In contrast, the model simulations at a 2.5-km resolution over the smaller domain using ISMC from the CRCM6-UAA simulation exhibit improved accuracy in capturing extreme events (group of blue scatters). These simulations accumulate the total amount of daily rainfall over the station very well compared to simulations at 12-km resolution (coral color scatters) and 2.5-km simulations using the initial land surface condition from the ERA5-Land dataset (green color scatters).

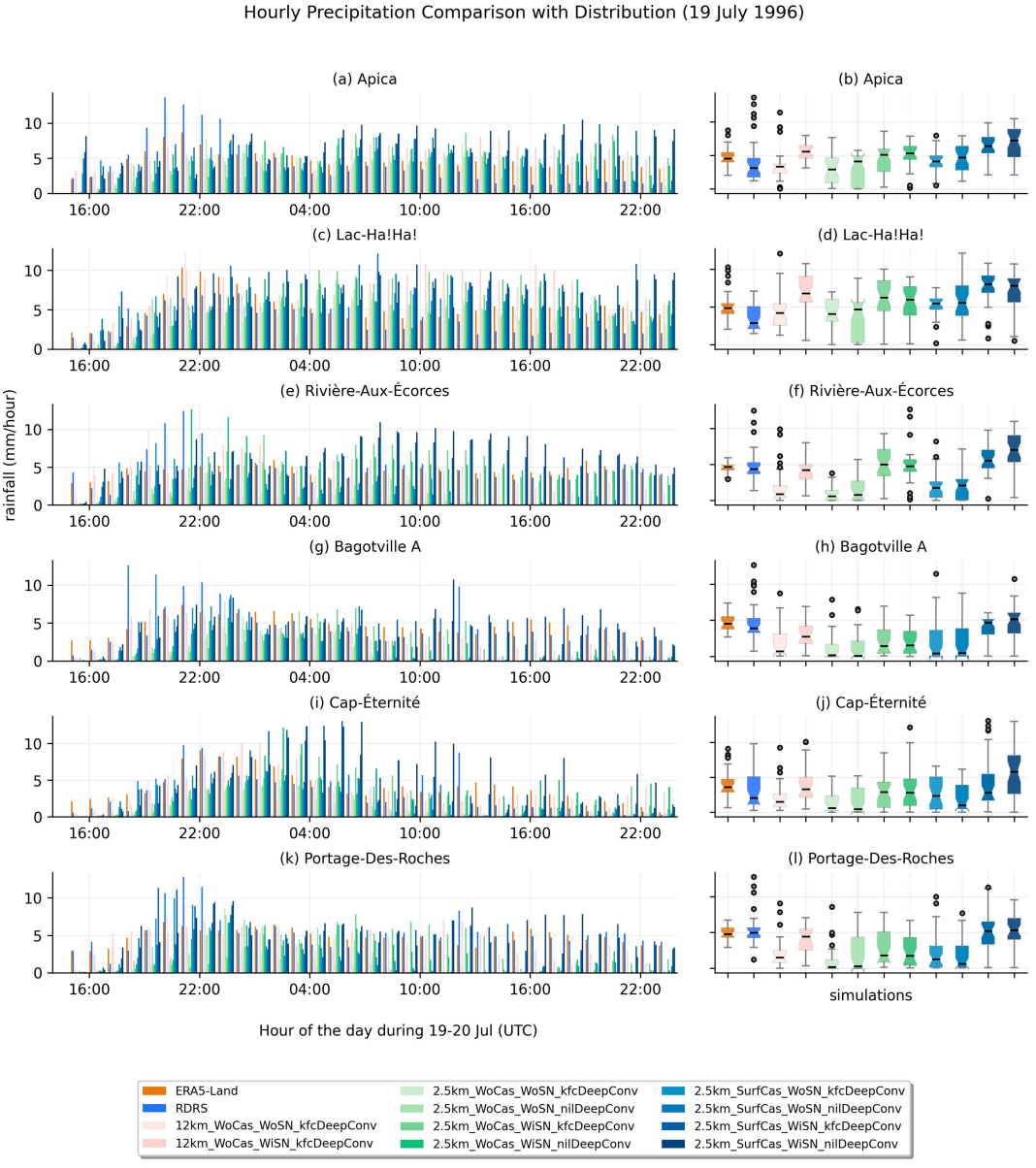

FIG. 10. (a)–(l) Hourly rainfall distribution at six different stations for 19–20 Jul 1996, with data distributions at the 25th and 75th percentiles, visualized using boxplots at a 95% confidence level for all the experiments from Table 2. The boxplots are constructed from 48 h of hourly precipitation data extracted over the grid points nearest to each station, as listed in Table 1. Different colored boxes within the boxplots represent the datasets, as indicated in the legend.

f. Hourly precipitation intensity and its characteristics

A comprehensive hourly rainfall pattern and the rainfall characteristics near the six weather stations (Table 1) can be observed from Figs. 10a–l. The station's hourly rainfall (mm h^{-1}) during 19–20 July 1996, along with the rainfall distribution of the respective stations, is visualized using boxplots at the 25th and 75th percentiles with a 95% confidence level. The arrival of the extreme event by the evening of 19 July is clearly visible over the six stations and continued throughout the next day, with heavy rainfall persisting overnight and into the late morning hours. Consistent heavy rainfall can be observed over the highland weather stations (refer to the bar diagram; Figs. 10a,c,e) (i.e., Apica, Lac-Ha! Ha!, and Rivière-Aux-Écorces) during the extreme event. In contrast, rainfall is comparatively less over the lowland weather stations (refer to the bar diagram; Figs. 10g,i,k) (i.e., Bagotville A, Cap-Éternité, and Portage-Des-Roches) later in the morning of 20 July. The model simulation follows the diurnal rainfall pattern from ERA5-Land and RDRS; however, while ERA5-Land and RDRS show a peak during the arrival of the extreme event, they record nearly half

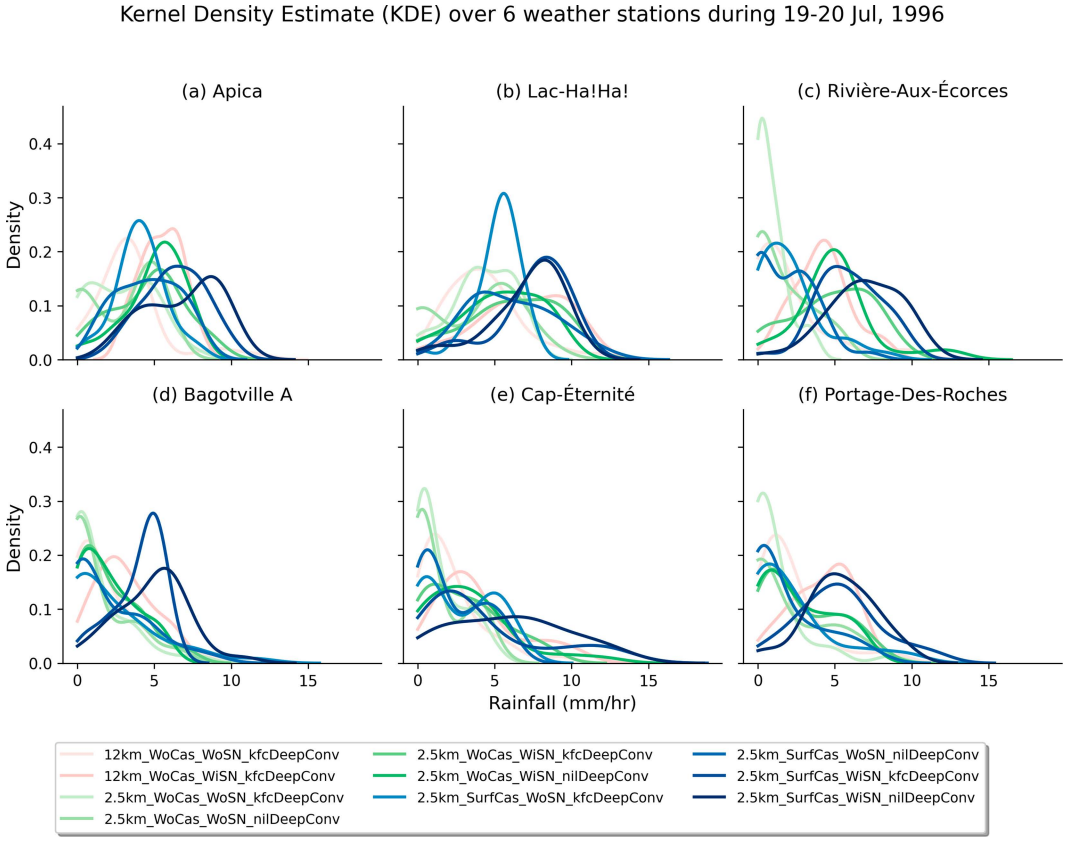

FIG. 11. (a)–(f) KDE of hourly precipitation over six different stations, based on 48 h of data at a 95% confidence interval, estimated (mm h^{-1}) during 19–20 Jul 1996 for all the experiments (experiment I–experiment X) from Table 2.

the hourly rainfall compared to the model afterward. The model shows intense rainfall using the model setup with a 2.5-km resolution and SN. It further shows high intensity in rainfall distribution while considering the ISMC from the CRCM6-UAA simulation. The median (Q2) and the interquartile range of the hourly rainfall distribution at the 25th (Q1) and 75th (Q3) percentiles demonstrate a wide range in hourly rainfall intensity at Q3 with a high central tendency (Q2) in most of the experiments over six weather stations (boxplots in Fig. 10). However, sharp peaks during certain hours helped maintain reasonable mean values and variability in the ERA5-Land and RDRS boxplots. Nonetheless, the hourly mean rainfall remains relatively low (e.g., Cavalleri et al. 2024, over Italy), which is consistent with the daily accumulation values shown in Table 3. The added value with SN at 12-km simulations shows an improvement in capturing the hourly rainfall pattern during the extreme event. However, the model simulations at 2.5-km resolution added more value in capturing the peak intensities during the extreme event in comparison with 12-km simulations. The added value from the 2.5-km resolution model simulation is quite impressive when applying SN while keeping CP activated. The ISMC from the CRCM6-UAA shows quite sensitive. The central tendency and interquartile range of the rainfall are quite high during the extreme event, with an approximation of 7 mm h^{-1} (e.g., Milbrandt and Yau 2001) over the highland area (refer to the boxplot; Figs. 10a–c) (i.e., Apica, Lac-Ha! Ha!, and Rivière-Aux-Écorces) and 5 mm h^{-1} over the lowland region (refer to the boxplot; Figs. 10d–f) (i.e., Bagotville A, Cap-Éternité, and Portage-Des-Roches). A maximum of 10–15 mm h^{-1} is observed during some hours using the simulation at 2.5-km resolution.

The KDE is calculated to visualize the distribution of rainfall, a continuous variable, at a 95% confidence level for each model simulation dataset presented in Figs. 11a–f. The figure reveals a wide spread across all datasets at all stations, extending up to 15 mm h^{-1}, highlighting the variability within the model-simulated data. While the most frequent values, central tendencies, and peak heights differ among datasets, a key observation is that the KDE can be categorized into two groups based on the use of SN. For the 12-km resolution data, SN results in a noticeable improvement in capturing rainfall intensity, as seen by a rightward shift in the central tendency. For the eight datasets at 2.5-km resolution, four distinct groups emerge. Group 1 includes data without SN, with or without CP, which follow similar KDE patterns. Group 2 comprises data with SN, with or without CP, showing either higher density or a rightward shift in the central tendency. Group 3 includes data without SN, with or without CP, and with ISMC from CRCM6-UAA, all of which follow a similar KDE pattern. Group 4

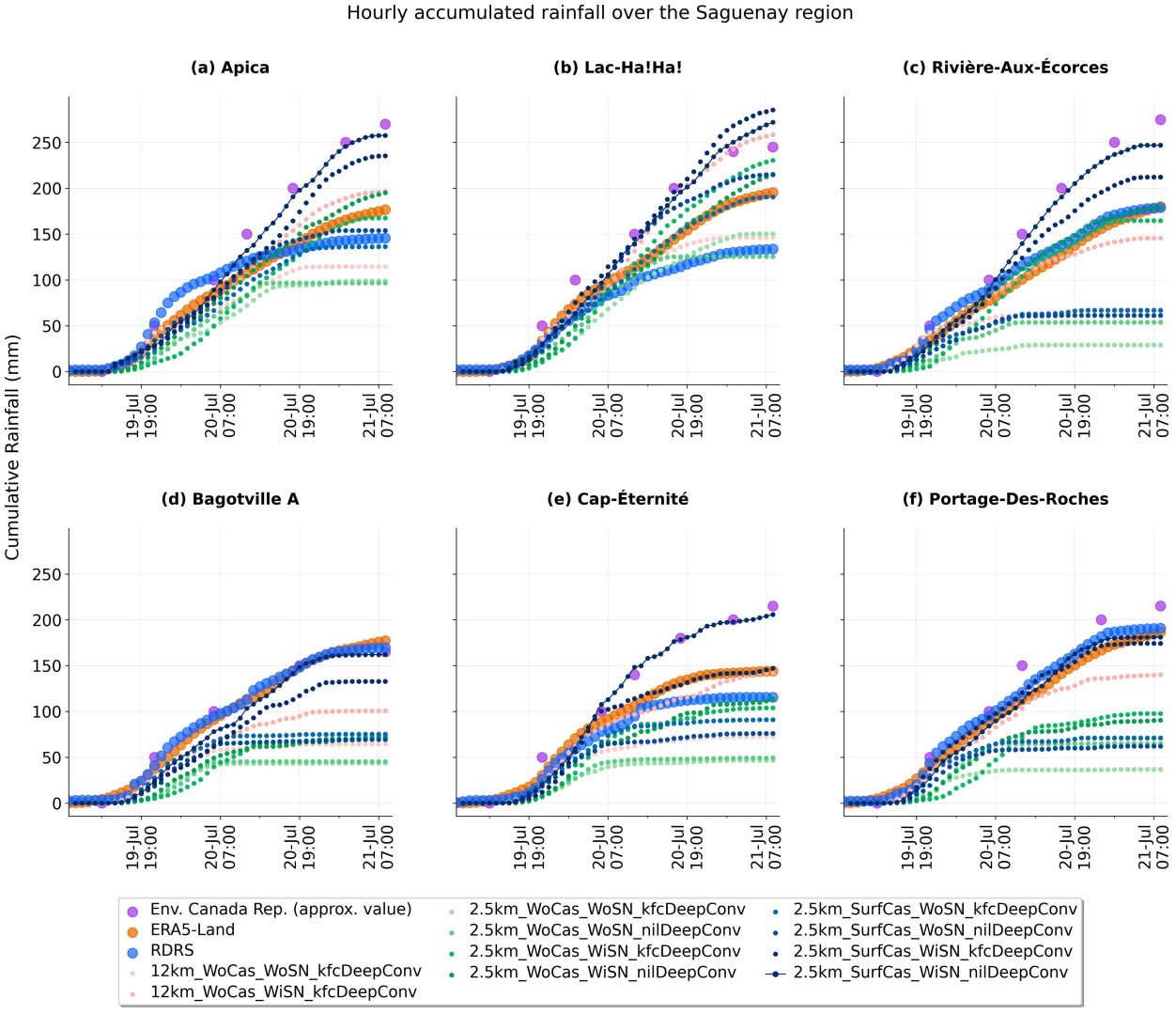

FIG. 12. (a)–(f) Hourly accumulated rainfall across various stations. The graph with larger scatter points represents data from station and reanalysis datasets, while the smaller scatter with a unique color represents the individual model simulation (experiment I–experiment X) detailed in Table 2. Hourly accumulation data for the ECCC report (scattered points in violet) are sourced from ECCC (1997), approximated from Fig. 19 (refer to Fig. S7 in the online supplemental material) of the respective report.

consists of data with SN, with or without CP, and with ISMC from CRCM6-UAA, showing a far-right shift in the KDE. Overall, the datasets form two main categories: one where all datasets except the last two (dark blue) have KDE peak positions between 0 and 5 mm h^{-1} and another where the remaining two datasets have peaks between 5 and 10 mm h^{-1}. Across the six stations, simulations with a 2.5-km resolution, ISMC from CRCM6-UAA, and SN show a rightward shift, with the KDE peak positioned between 5 and 10 mm h^{-1}. Notably, the model setup with CP off draws further attention by exhibiting a more pronounced rightward shift in the KDE peak position.

g. Hourly cumulative rainfall simulation at stations

The hourly accumulated rainfall over the region is of significant interest to researchers and stakeholders aiming to understand the key areas of concern (e.g., timing, intensity, localization, daily accumulation of rainfall) during the extreme event like Saguenay 1996 (e.g., ECCC 1997; Milbrandt and Yau 2001). In Fig. 12, the larger scatter points correspond to data from station and reanalysis datasets, while the smaller, multicolored scatter points represent various simulations outlined in Table 2.

Analyzing the stations and the surrounding topography reveals that the first three weather stations Apica, Lac-Ha! Ha!, and Rivière-Aux-Écorces are located in highland regions (Figs. 12a–c), while the remaining three weather stations Bagotville A, Cap-Éternité, and Portage-Des-Roches are situated in lowland/plain (Figs. 12d–f). Stations in the highland or foothill regions received high rainfall intensity and reached the total accumulated rainfall of approximately 250 mm, following the ECCC report data (Figs. 12a–c). This can be attributed to the elevation and the geographic position of the region

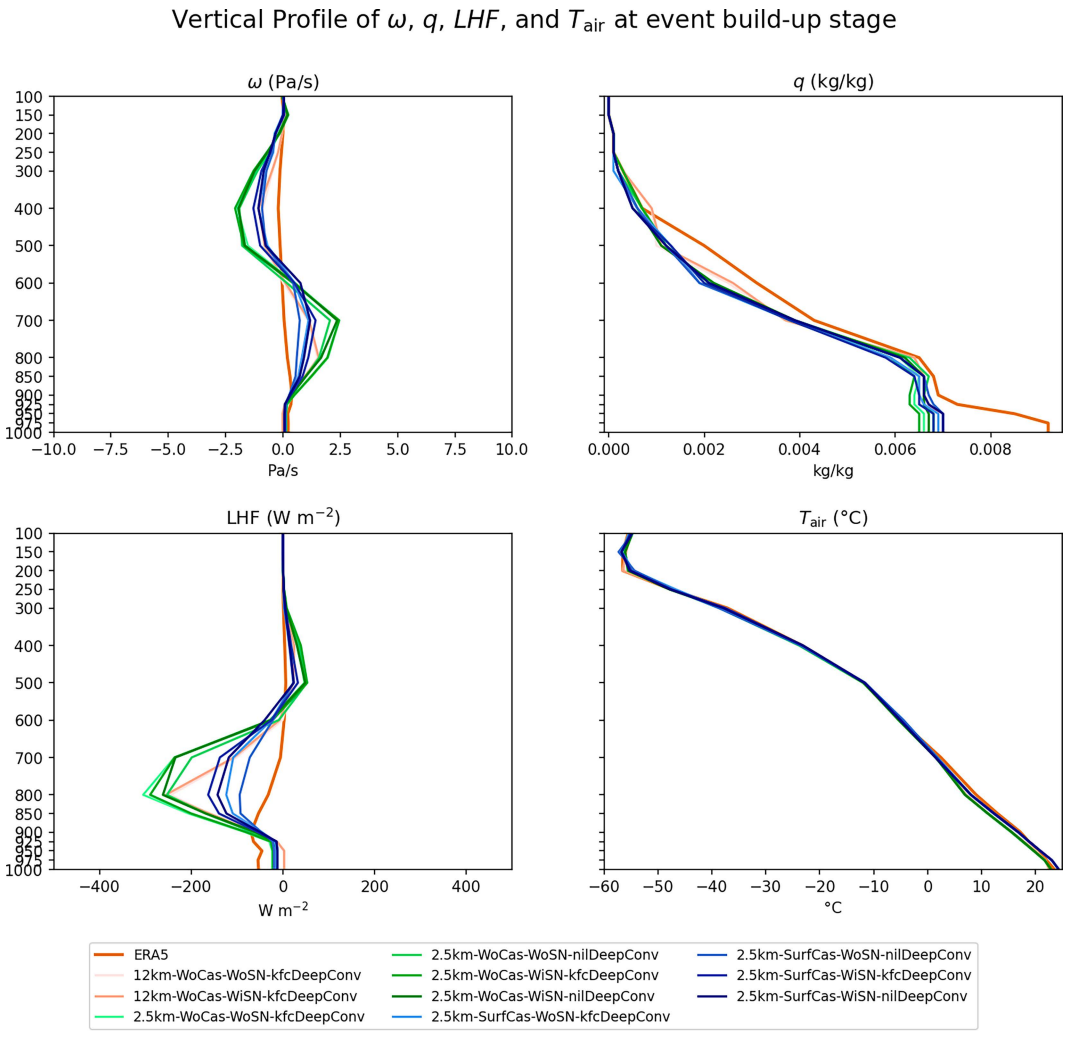

FIG. 13. Vertical profiles of omega ω (Pa s^{-1}), specific humidity q (kg kg^{-1}), LHF (W m^{-2}), and air temperature T_{air} (°C) at the extreme event buildup stage (0000 UTC 19 Jul 1996) over a high rainfall zone (48°N and 70.4°W).

(Milbrandt and Yau 2001). The sharp peak in the hourly accumulated rainfall during extreme precipitation events is evident from the first three stations, and the model simulations capture the rainfall pattern during this period. However, most simulations fail to capture the peak rainfall intensity observed in the station data. The ERA5-Land and RDRS datasets significantly underestimate the station rainfall data in highland areas.

Moreover, stations located in plain regions received less rainfall (Figs. 12d–f) compared to highland stations. The reason behind this rainfall pattern over the plains could be on losses of energy by late morning on 20 July, which is further stabilized by the evening. This gradual increase followed by a decrease in hourly accumulated rainfall is also well captured. The scatters in deep blue show a close estimation of the station rainfall data from the ECCC report. The CPM at 2.5-km resolution provides more accurate rainfall estimates by closely following the station rainfall data from the ECCC report. The simulation without convection parameterization using SN and ISMC from the CRCM6-UAA simulation further provides the most accurate estimates of hourly accumulated rainfall. In plain regions, the ERA5-Land and RDRS datasets provide estimates close to the station rainfall data.

4. Physical process and evolution of synoptic features in model simulations

The physical process of the Saguenay flood extreme event buildup stage (0000 UTC 19 July 1996) over a high rainfall zone (48°N and 70.4°W) is shown in Fig. 13. Upward motion (negative ω) indicates large-scale lifting, necessary to trigger deep convection. Prior to an extreme precipitation event, ω typically becomes strongly negative between 700 and 400 hPa, reflecting synoptic-scale forcing. ERA5 shows weak upward motion in the midlevels, inconsistent with prestorm lift. The 12-km runs simulate weaker ascent, likely due to coarse resolution and parameterized convection. The 2.5 km with ERA5-Land ISMC, with SN, and without deep convection parameterization shows stronger ascent. CRCM6-UAA soil

configurations, especially with and without SN along without deep convection parameterization, match ERA5 best, indicating that realistic large-scale lifting is better captured when the deep convection parameterization is turned off. High specific humidity q in the lower troposphere (from the surface to ~700 hPa) is essential for convective development before the extreme event. A steep vertical gradient (moist below, dry aloft) indicates potential instability, fueling latent heat release during ascent. ERA5 exhibits a surface q of $\sim$ 0.008 kg kg^{-1}, with a sharp decline upward. The 12-km and some 2.5-km simulations with active deep convection parameterization tend to underestimate near-surface air moisture, which can dampen convective potential. Simulations with CRCM6-UAA ISMC, with SN, and without deep convection parameterization at 2.5 km retain higher near-surface q values, better representing prestorm moisture buildup. These configurations simulate realistic instability through proper moisture vertical gradients, necessary to trigger heavy rainfall later. The strong negative LHF values (~ -300 kg m^{-2}) around 800 hPa in the 12-km and some 2.5-km simulations with deep convection parameterization reflect premature convection triggering. This leads to midlevel drying and stabilization, evident in subsidence-dominated LHF profiles. These configurations fail to sustain moist instability, limiting their ability to simulate realistic convection buildup (Helms and Bosart 2021). Additionally, ERA5 exhibits lower LHF values near the surface, indicating reduced upward moisture transport from the surface. This suggests that weaker moisture advection in the atmospheric boundary layer may have led to suppressed surface evaporation, contributing to lower LHF. The 2.5-km simulations with CRCM6-UAA ISMC with no deep convection parameterization show higher positive LHF values near the surface compared to other configurations. This prevents premature atmospheric stabilization, allowing convection to be sustained longer and grow deeper. The simulations with 2.5 km with CRCM6-UAA ISMC and without deep convection parameterization (with and without SN) exhibit the strongest upward latent heat flux, especially below 850–900 hPa. However, further work is needed to have a detailed understanding. A lapse rate (cooling with height) provides potential for vertical motion and storm growth. Surface heating enhances instability when paired with soil moisture. The temperature structure is well captured across the region, even by coarser models. However, simulations at 2.5 km and CRCM6-UAA ISMC display similar T_{air} profiles as ERA5.

Given its performance, the 2.5-km CRCM6-UAA ISMC simulation with SN and without deep convection is selected to assess the model's capability in capturing the evolution of synoptic features and the storm track, as presented in Fig. 14. This figure mirrors the ERA5-based analysis shown in Fig. 1. On 1800 UTC 19 July, a developing low pressure system was located south of Quebec, with wind patterns at 850 hPa indicating initial convergence and strengthening in the lower atmosphere. Simultaneously (Fig. 14a), the 500-hPa level showed early signs of moisture convergence, highlighted by the VIMD field, and a developing upper-level trough that provided the necessary dynamical support for upward motion (Fig. 14b). By 0600 UTC 20 July, the system had intensified further, with the surface low deepening and shifting northeast (Fig. 14c). The 850-hPa wind speeds increased, enhancing moisture transport into the region (Fig. 14d). At the same time, a more pronounced gradient in VIMD indicated stronger moisture convergence columns [whereas the CRCM6 reveals localized divergence associated with explicitly resolved downdrafts and outflows, which is often absent in coarser and parameterized system (e.g., Groot et al. 2024)], along with more heterogeneity in divergence/convergence over land/oceanic regions. The trough at 500 hPa became more amplified, further supporting upward vertical motion and precipitation development. By 0000 UTC 21 July, the low pressure system had fully intensified over Quebec (Fig. 14e). High wind speeds at 850 hPa and continued convergence contributed to sustained moisture inflow (Fig. 14f). At the 500-hPa level, tightly packed geopotential height contours and a concentrated center of strong VIMD signaled vigorous dynamic lifting and peak moisture convergence, setting the stage for maximum rainfall. The key processes that led to the flooding included surface cyclogenesis, which drew moist air from the south; strong moisture convergence, especially on 20 and 21 July, and robust upper-level support from a deep trough. Wind convergence at the lower levels further enhanced rising motion, and the storm's slow movement over Quebec resulted in prolonged and intense rainfall. These combined factors ultimately led to severe soil saturation and the catastrophic flooding experienced during the event.

5. Discussion

Current studies have found that SN in climate models is crucial due to its ability to follow imposed large-scale patterns from driving models (ERA5/GCM) and minimize the discrepancies between model outputs and observational data (von Storch et al. 2000). By focusing on the role of SN in climate model performance, an improved understanding of timing, intensity, and localization is shown when using the RCM for the Saguenay 1996 flood extreme event simulation.

Our analysis has shown that the 12-km resolution and ERA5-Land initial and boundary conditions are not able to accurately reproduce the rainfall over the region. However, when using the SN setup, the model shows some improvement in reproducing the rainfall amounts over the plain and highland regions. Yet, the model still falls short of matching the observed rainfall data from the weather stations and exhibits a lack in simulated rainfall. The differences in spatial and temporal rainfall patterns between the observed and/or reanalysis data at the weather stations and the model simulation at 12-km resolution underscore the importance of a fine-scale modeling approach where the physical processes involved in the CPMs are accurately simulating extreme weather events and providing reliable precipitation quantities for flood-prone regions such as Saguenay.

The 2.5-km resolution shows the most accurate estimates of hourly accumulated rainfall by capturing the highest rainfall intensity including the timing intensity characteristics during extreme precipitation events regardless of topography. Previous studies

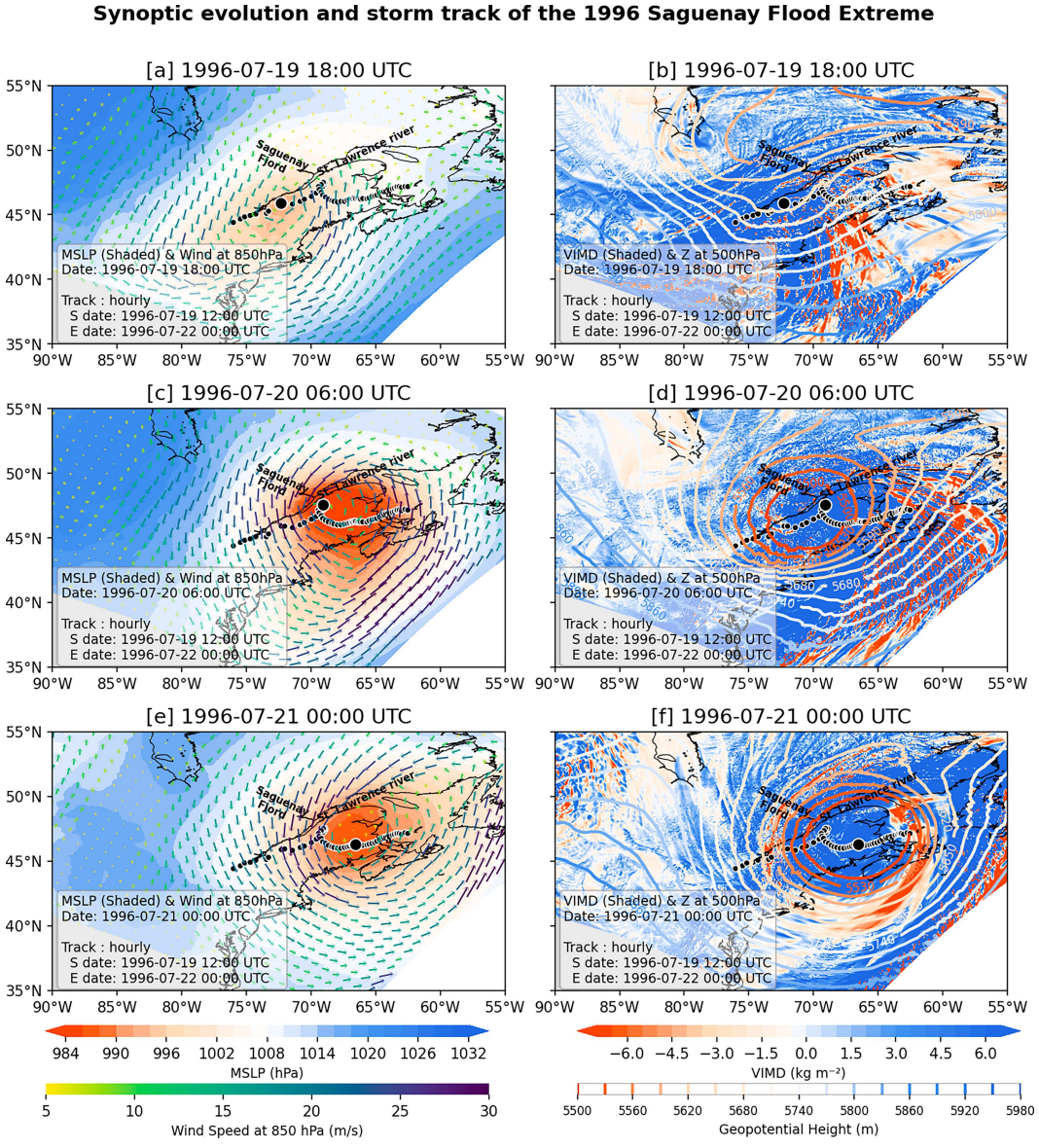

FIG. 14. Synoptic storm-track features at (a),(b) 1800 UTC 19 Jul, (c),(d) 0600 UTC 20 Jul, and (e),(f) 0000 UTC 21 Jul 1996 based on the CRCM6 simulation at 2.5-km resolution with SN and CRCM6-UAA ISMCs (Table 2; experiment X) (as in Fig. 1). (a),(c),(e) MSLP (hPa) and 850-hPa wind vectors (m s^{-1}). (b),(d),(f) VIMD (kg m^{-2}) and 500-hPa geopotential height (m). The storm track is overlaid in each panel using hourly minimum MSLP points from 1200 UTC 19 Jul to 0000 UTC 22 Jul. The large black point in each panel indicates the storm's position at the respective hour of that panel.

have emphasized the limitations of gridded datasets produced by models using deep convection parameterizations in capturing localized extreme rainfall events. For example, Fosser et al. (2024) discuss the challenges in accurately simulating extremes due to the spatial variability of rainfall patterns, which can significantly impact the reliability of flood simulations (e.g., Ferrett et al. 2021). The study highlights that the CRCM6 model performs better with SN, as the CPM setup enhances the simulation of extreme events. The CP setup, where deep convection parameterization is off, is particularly more reliable in capturing peak rainfall intensity and also the timing of intensity during such events. By showing similar results whether the KFC scheme is activated or deactivated, the CPM resolves convection parameterization independently over the region (e.g., Prein et al. 2017). However, when the deep convection parameterization is turned off in CP mode, the model improves rainfall intensity for capturing extreme precipitation events. Over 2 consecutive days, simulations with this setup either match or closely align with observed station rainfall data. Complex topography limits the ability of reanalysis datasets to capture actual rainfall

over the weather stations, especially in highland regions. Model simulations at 2.5-km resolution offer more accurate rainfall estimates compared to the ERA5-Land, RDRS, and 12-km simulations, in terms of both amount and intensity of observed station rainfall. However, the limited availability of the observed data from these areas and time periods hinders the comprehensive assessment of extreme weather events.

By comparing simulations with ERA5 initial and boundary conditions to simulations using ISMC from the CRCM6-UAA simulation, we have observed significant increases in rainfall amounts and better spatial patterns, particularly in regions such as the highland region and the bay. Excessive soil moisture, as depicted in Fig. 3a with ISMC from ERA5-Land, leads to an underestimation of rainfall with CRCM6. Moreover, drier land at the beginning of a simulation, illustrated in Fig. 3b using ISMC from the CRCM6-UAA simulation, results in an overestimation of rainfall with CRCM6. This soil moisture–precipitation feedback mechanism can be explained through dynamic soil–atmosphere feedback, atmospheric humidity, convection and precipitation, and model calibration (Brimelow and Reuter 2005; Hohenegger et al. 2009; Uber et al. 2018). Soil moisture is crucial for the exchange of water and energy between the land surface and the atmosphere. Low soil moisture reduces water availability for evaporation and transpiration, leading to decreased atmospheric humidity. While this initially results in less cloud formation, it also reduces the suppression of convection, thereby increasing atmospheric instability. This instability leads to more intense convective activity and heavier precipitation when the Saguenay 1996 system passes through. During model calibration, low ISMCs cause the climate model to show wet conditions by generating higher rainfall to balance the water cycle. Furthermore, we have noticed that the CPMs also exhibit sensitivity to ISMC, further emphasizing the importance of accurate surface data in this configuration.

The above analyses demonstrate that SN and ISMCs in the CPM setup significantly improve the accuracy of precipitation extremes, particularly over the northern bay and highland regions, by refining climate models and enhancing the representation of extreme weather events. The model shows a similar level of sensitivity when using ISMCs as with the SN setup.

6. Conclusions

This work aims to identify an optimal configuration of the CRCM6 convection-permitting (CP) regional climate model (RCM) for studying precipitation extremes. To achieve this, one of Canada's most catastrophic case studies, the 1996 Saguenay flood, is considered due to its significant impact on Canada's climate change history. The study demonstrates the simulation of precipitation extremes and rainfall patterns on hourly and daily time scales through the use of spectral nudging (SN) in convection-permitting models (CPMs) and the importance of the ISMC to have an optimal CPM configuration.

Hourly Rainfall Measurements: Analysis of hourly rainfall during the extreme event across various weather stations (Apica, Lac-Ha! Ha!, Rivière-Aux-Écorces, Bagotville A, Cap-Éternité, and Portage-Des-Roches) reveals that the 2.5-km resolution CPM setup significantly improves the accuracy of rainfall simulation. Simulations using ISMC from CRCM6-UAA and SN show a central tendency with a KDE peak between 5 and 10 mm h^{-1}. The CPM configuration without deep convection effectively captures the spatial distribution of rainfall on a daily time scale when compared to weather station observations.

Hourly Accumulated Rainfall: The 2.5-km resolution model setup accurately captures hourly accumulation compared to observed rainfall. In regions like the Laurentian and Charlevoix Mountains, the model provides more accurate rainfall estimates than ERA5-Land and RDRS reanalysis, which fail to match observed accumulations at weather stations.

SN Enhancements: Adjustments to the SN technique, such as applying a spectral space filter (200 km for small scale and 900 km for large scale), using a cosine-squared function for the vertical profile starting at hybrid level 0.7 (which is approximately 700 hPa), setting an 8-h relaxation time scale, adjusting the nudging interval to 60 s, and disabling nudging weight in temporal space, have significantly improved the timing, intensity, and spatial pattern of precipitation in CRCM6 simulations.

Soil Moisture Modification: The use of ISMC demonstrates a strong sensitivity in the model's performance. Specifically, ISMC from the 12-km CRCM6-UAA appears to influence the model's ability to reproduce extreme rainfall patterns. This sensitivity is comparable to that observed with SN, highlighting the critical role of realistic soil data in simulating rainfall extremes.

Further, the study highlights the efficacy of the 2.5-km resolution CPM setup in simulating extreme precipitation events, particularly in regions with complex topographies. The use of SN and reliable ISMC can significantly improve the model's performance. The CPM setup's ability to independently resolve convection without parameterization allows for a more accurate representation of rainfall patterns and intensities.

While the 2.5-km resolution model provides significant improvements, the study acknowledges limitations in gridded rainfall datasets like ERA5-Land and RDRSv2.1, which often underestimate rainfall in regions with steep slopes and deep valleys. These limitations must be considered in future extreme precipitation analyses and flood management strategies.

The study concludes that the CPM setup at 2.5-km resolution offers clear added value in simulating extreme precipitation events, particularly in complex topographies. The combination of SN and realistic ISMC can enhance the model's ability to replicate observed rainfall patterns. However, the current modeling framework has key limitations. Its ability to test diverse soil conditions is restricted when using the CLASS land surface scheme. The 2.5-km grid spacing limits fine-scale process resolution, and a 1-km grid could offer improvements. Running simulation ensembles would help assess internal variability. Hindcast-mode setup, as in ECCC forecasts, may aid model evaluation. A full diagnostic of surface moisture and its impacts on the water cycle budget still remains an open question.

Acknowledgments. We sincerely thank the three anonymous reviewers and the editor for their valuable comments and constructive feedback that helped improve the quality of this manuscript. We acknowledge the financial support from the Natural Sciences and Engineering Research Council of

Canada (NSERC) through the Alliance Grant (576492-2022) obtained by Prof. Philippe Gachon. The authors wish to express their gratitude to Dr. Katja Winger for her invaluable support in the model upgrade and computational assistance and Mr. François Roberge for his support in different stages of model setup. The authors also extend their appreciation to Hydro-Québec, partners in the mining sector, and the Ministère de l'Environnement et de la Lutte contre les Changements Climatiques, de la Faune et des Parcs (MELCCFP) du Québec for their financial support. The computational facilities were provided by Calcul Canada under the Digital Research Alliance of Canada.

Data availability statement. The simulated data that support the findings of this study are available from the corresponding author upon reasonable request.

REFERENCES

Alexandru, A., R. De Elia, R. Laprise, L. Separovic, and S. Biner, 2009: Sensitivity study of regional climate model simulations to large-scale nudging parameters. *Mon. Wea. Rev.*, **137**, 1666–1686, https://doi.org/10.1175/2008MWR2620.1.

Asif, Z., and Z. Chen, 2016: Environmental management in North American mining sector. *Environ. Sci. Pollut. Res.*, **23**, 167–179, https://doi.org/10.1007/s11356-015-5651-8.

Ban, N, and Coauthors, 2021: The first multi-model ensemble of regional climate simulations at kilometer-scale resolution, part I: Evaluation of precipitation. *Climate Dyn.*, **57**, 275–302, https://doi.org/10.1007/s00382-021-05708-w.

Bechtold, P., E. Bazile, F. Guichard, P. Mascart, and E. Richard, 2001: A mass-flux convection scheme for regional and global models. *Quart. J. Roy. Meteor. Soc.*, **127**, 869–886, https://doi.org/10.1002/qj.49712757309.

Bélair, S., L.-P. Crevier, J. Mailhot, B. Bilodeau, and Y. Delage, 2003a: Operational implementation of the ISBA land surface scheme in the Canadian regional weather forecast model. Part I: Warm season results. *J. Hydrometeor.*, **4**, 352–370, https://doi.org/10.1175/1525-7541(2003)4<352:OIOTIL>2.0.CO;2.

——, R. Brown, J. Mailhot, B. Bilodeau, and L.-P. Crevier, 2003b: Operational implementation of the ISBA land surface scheme in the Canadian regional weather forecast model. Part II: Cold season results. *J. Hydrometeor.*, **4**, 371–386, https://doi.org/10.1175/1525-7541(2003)4<371:OIOTIL>2.0.CO;2.

——, J. Mailhot, C. Girard, and P. Vaillancourt, 2005: Boundary layer and shallow cumulus clouds in a medium-range forecast of a large-scale weather system. *Mon. Wea. Rev.*, **133**, 1938–1960, https://doi.org/10.1175/MWR2958.1.

Belušić, A., M. T. Prtenjak, I. Güttler, N. Ban, D. Leutwyler, and C. Schär, 2018: Near-surface wind variability over the broader Adriatic region: Insights from an ensemble of regional climate models. *Climate Dyn.*, **50**, 4455–4480, https://doi.org/10.1007/s00382-017-3885-5.

Benoit, C., I. Demers, F. Roberge, P. Gachon, and R. Laprise, 2022: Inondations des printemps 2017 et 2019 dans le Bassin versant de la rivière des Outaouais (Québec, Canada): Analyse des facteurs physiographiques et météorologiques en cause. *Les Inondations au Québec: Risques, Aménagement du Territoire, Impacts Socioéconomiques et Transformation des Vulnérabilités*, T. Buffin-Bélanger, D. Maltais, and M. M. Gauthier, Eds., Presse de l'Université du Québec, 29–58.

Biner, S. D. Caya, R. Laprise, and L. Spacek, 2000: Nesting of RCMS by imposing large scales. Research activities in atmospheric and oceanic modelling. WMO/TD-987 30, 7.3–7.4.

Bowden, J. H., T. L. Otte, C. G. Nolte, and M. J. Otte, 2012: Examining interior grid nudging techniques using two-way nesting in the WRF model for regional climate modeling. *J. Climate*, **25**, 2805–2823, https://doi.org/10.1175/JCLI-D-11-00167.1.

Brimelow, J. C., and G. W. Reuter, 2005: Transport of atmospheric moisture during three extreme rainfall events over the Mackenzie River basin. *J. Hydrometeor.*, **6**, 423–440, https://doi.org/10.1175/JHM430.1.

Burn, D. H., and P. H. Whitfield, 2016: Changes in floods and flood regimes in Canada. *Can. Water Resour. J.*, **41**, 139–150, https://doi.org/10.1080/07011784.2015.1026844.

Bush, E., and D. S. Lemmen, Eds., 2019: *Canada's Changing Climate Report.* Government of Canada, 444 pp., https://changingclimate.ca/CCCR2019/.

Cavalleri, F., and Coauthors, 2024: Multi-scale assessment of high-resolution reanalysis precipitation fields over Italy. *Atmos. Res.*, **312**, 107734, https://doi.org/10.1016/j.atmosres.2024.107734.

ECCC, 1997: Pluies diluviennes du 18 au 21 Juillet 1996, au Québec: Analyse et interprétation de données Météorologiques et climatologiques. Ministre des Approvisionnements et Services de catalogue: En56-122/2-1997F, 110 pp, https://www.cubiq.ribg.gouv.qc.ca/notice?id=p%3A%3Ausmarcdef_0000474449&locale=fr.

——, 2024: Historical climate data, Climate normals for Bagotville, Québec (Canada). https://climat.meteo.gc.ca/climate_normals/results_1981_2010_f.html?stnID=5889&autofwd=1.

Endris, H. S., and Coauthors, 2013: Assessment of the performance of CORDEX regional climate models in simulating East African rainfall. *J. Climate*, **26**, 8453–8475, https://doi.org/10.1175/JCLI-D-12-00708.1.

Faucher, G., 2002: Les coûts économiques de catastrophes récentes subies par le Québec. Institut de la Statistique Québec, 11 pp, https://numerique.banq.qc.ca/patrimoine/details/52327/50991.

Ferrett, S., T. H. A. Frame, J. Methven, C. E. Holloway, S. Webster, T. H. M. Stein, and C. Cafaro, 2021: Evaluating convection-permitting ensemble forecasts of precipitation over Southeast Asia. *Wea. Forecasting*, **36**, 1199–1217, https://doi.org/10.1175/WAF-D-20-0216.1.

Feser, F., and M. Barcikowska, 2012: The influence of spectral nudging on typhoon formation in regional climate models. *Environ. Res. Lett.*, **7**, 014024, https://doi.org/10.1088/1748-9326/7/1/014024.

Fosser, G., and Coauthors, 2024: Convection-permitting climate models offer more certain extreme rainfall projections. *npj Climate Atmos. Sci.*, **7**, 51, https://doi.org/10.1038/s41612-024-00600-w.

Funk, T., 2011: A practical, basic guide to quasi-geostrophic theory: Response to geostrophic deformation, ageostrophic motion and jet streaks. NWS Tech. Rep., 26 pp., https://www.weather.gov/media/lmk/soo/QG_Theory_Review.pdf.

Gasset, N., and Coauthors, 2021: A 10 km North American precipitation and land-surface reanalysis based on the GEM atmospheric model. *Hydrol. Earth Syst. Sci.*, **25**, 4917–4945, https://doi.org/10.5194/hess-25-4917-2021.

Gillett, N. P., and Coauthors, 2022: Human influence on the 2021 British Columbia floods. *Wea. Climate Extremes*, **36**, 100441, https://doi.org/10.1016/j.wace.2022.100441.

Giorgi, F., and W. J. Gutowski Jr., 2015: Regional dynamical downscaling and the CORDEX initiative. *Annu. Rev. Environ.*

Resour., **40**, 467–490, https://doi.org/10.1146/annurev-environ-102014-021217.

Groot, E., P. Kuntze, A. Miltenberger, and H. Tost, 2024: Divergent convective outflow in ICON deep-convection-permitting and parameterised deep convection simulations. *Wea. Climate Dyn.*, **5**, 779–803, https://doi.org/10.5194/wcd-5-779-2024.

Gutowski, W. J., Jr., and Coauthors, 2020: The ongoing need for high-resolution regional climate models: Process understanding and stakeholder information. *Bull. Amer. Meteor. Soc.*, **101**, E664–E683, https://doi.org/10.1175/BAMS-D-19-0113.1.

Helms, C. N., and L. F. Bosart, 2021: The impact of a midlevel dry airflow layer on deep convection in the pre-Gabrielle (2013) tropical disturbance on 4–5 September. *Mon. Wea. Rev.*, **149**, 2695–2711, https://doi.org/10.1175/MWR-D-20-0380.1.

Hentgen, L., N. Ban, N. Kröner, D. Leutwyler, and C. Schär, 2019: Clouds in convection-resolving climate simulations over Europe. *J. Geophys. Res. Atmos.*, **124**, 3849–3870, https://doi.org/10.1029/2018JD030150.

Hersbach, H., and Coauthors, 2020: The ERA5 global reanalysis. *Quart. J. Roy. Meteor. Soc.*, **146**, 1999–2049, https://doi.org/10.1002/qj.3803.

Hohenegger, C., P. Brockhaus, C. S. Bretherton, and C. Schär, 2009: The soil moisture–precipitation feedback in simulations with explicit and parameterized convection. *J. Climate*, **22**, 5003–5020, https://doi.org/10.1175/2009JCLI2604.1.

Holton, J. R., and G. J. Hakim, 2013: *An Introduction to Dynamic Meteorology*. International Geophysics Series, Vol. 88, Academic Press, 532 pp.

Hydro-Québec, 2022: Climate Change Adaptation Plan 2022–2024. Hydro-Québec, 132 pp, https://www.hydroquebec.com/themes/plan-adaptation-changements-climatiques/pdf/pg-1037-2022g344a-pacc-v02a.pdf.

IPCC, 2023: *Climate Change 2023: Synthesis Report.* IPCC, 184 pp., https://doi.org/10.59327/IPCC/AR6-9789291691647.

Kain, J. S., and J. M. Fritsch, 1990: A one-dimensional entraining/detraining plume model and its application in convective parameterization. *J. Atmos. Sci.*, **47**, 2784–2802, https://doi.org/10.1175/1520-0469(1990)047<2784:AODEPM>2.0.CO;2.

Kendon, E., A. F. Prein, C. Senior, and A. Stirling, 2021: Challenges and outlook for convection-permitting climate modelling. *Philos. Trans. Roy. Soc.*, **A379**, 20190547, https://doi.org/10.1098/rsta.2019.0547.

Lin, C. A., L. Wen, M. Béland, and D. Chaumont, 2002: A coupled atmospheric-hydrological modeling study of the 1996 Ha! Ha! River basin flash flood in Québec, Canada. *Geophys. Res. Lett.*, **29**, 1026, https://doi.org/10.1029/2001GL013827.

Llerena, A., P. Gachon, and R. Laprise, 2023: Precipitation extremes and their links with regional and local temperatures: A case study over the Ottawa River Basin, Canada. *Atmosphere*, **14**, 1130, https://doi.org/10.3390/atmos14071130.

Lucas-Picher, P., D. Caya, R. de Elía, and R. Laprise, 2008: Investigation of regional climate models' internal variability with a ten-member ensemble of 10-year simulations over a large domain. *Climate Dyn.*, **31**, 927–940, https://doi.org/10.1007/s00382-008-0384-8.

——, D. Argüeso, E. Brisson, Y. Tramblay, P. Berg, A. Lemonsu, S. Kotlarski, and C. Caillaud, 2021: Convection -permitting modeling with regional climate models: Latest developments and next steps. *Wiley Interdiscip. Rev.: Climate Change*, **12**, e731, https://doi.org/10.1002/wcc.731.

Lüthi, S., N. Ban, S. Kotlarski, C. R. Steger, T. Jonas, and C. Schär, 2019: Projections of Alpine snow-cover in a high-resolution climate simulation. *Atmosphere*, **10**, 463, https://doi.org/10.3390/atmos10080463.

Maltais, D., S. Robichaud, and A. Simard, 1999: *The July 1996 Saguenay Disaster: Impacts on Redefining the Habitat.* Université du Québec à Chicoutimi, 173 pp.

McTaggart-Cowan, R., and Coauthors, and, 2019: Modernization of atmospheric physics parameterization in Canadian NWP. *J. Adv. Model. Earth Syst.*, **11**, 3593–3635, https://doi.org/10.1029/2019MS001781.

Miguez-Macho, G., G. L. Stenchikov, and A. Robock, 2004: Spectral nudging to eliminate the effects of domain position and geometry in regional climate model simulations. *J. Geophys. Res.*, **109**, D13104, https://doi.org/10.1029/2003JD004495.

——, ——, and ——, 2005: Regional climate simulations over North America: Interaction of local processes with improved large-scale flow. *J. Climate*, **18**, 1227–1246, https://doi.org/10.1175/JCLI3369.1.

Milbrandt, J. A., and M. K. Yau, 2001: A mesoscale modeling study of the 1996 Saguenay flood. *Mon. Wea. Rev.*, **129**, 1419–1440, https://doi.org/10.1175/1520-0493(2001)129<1419:AMMSOT>2.0.CO;2.

Muñoz-Sabater, J., and Coauthors, 2021: ERA5-land: A state-of-the-art global reanalysis dataset for land applications. *Earth Syst. Sci. Data*, **13**, 4349–4383, https://doi.org/10.5194/essd-13-4349-2021.

Noilhan, J., and S. Planton, 1989: A simple parameterization of land surface processes for meteorological models. *Mon. Wea. Rev.*, **117**, 536–549, https://doi.org/10.1175/1520-0493(1989)117<0536:ASPOLS>2.0.CO;2.

——, and J.-F. Mahfouf, 1996: The ISBA land surface parameterisation scheme. *Global Planet. Change*, **13**, 145–159, https://doi.org/10.1016/0921-8181(95)00043-7.

Pichelli, E., and Coauthors, 2021: The first multi-model ensemble of regional climate simulations at kilometer-scale resolution part 2: Historical and future simulations of precipitation. *Climate Dyn.*, **56**, 3581–3602, https://doi.org/10.1007/s00382-021-05657-4.

Prein, A. F., and Coauthors, 2015: A review on regional convection-permitting climate modeling: Demonstrations, prospects, and challenges. *Rev. Geophys.*, **53**, 323–361, https://doi.org/10.1002/2014RG000475.

——, R. Rasmussen, and G. Stephens, 2017: Challenges and advances in convection-permitting climate modeling. *Bull. Amer. Meteor. Soc.*, **98**, 1027–1030, https://doi.org/10.1175/BAMS-D-16-0263.1.

Rasmussen, R., and Coauthors, 2011: High-resolution coupled climate runoff simulations of seasonal snowfall over Colorado: A process study of current and warmer climate. *J. Climate*, **24**, 3015–3048, https://doi.org/10.1175/2010JCLI3985.1.

Roberge, F., A. Di Luca, R. Laprise, P. Lucas-Picher, and J. Thériault, 2024: Spatial spin-up of precipitation in limited-area convection-permitting simulations over North America using the CRCM6/GEM5.0 model. *Geosci. Model Dev.*, **17**, 1497–1510, https://doi.org/10.5194/gmd-17-1497-2024.

Rockel, B., and B. Geyer, 2008: The performance of the regional climate model CLM in different climate regions, based on the example of precipitation. *Meteor. Z.*, **17**, 487–498, https://doi.org/10.1127/0941-2948/2008/0297.

Schaefli, B., R. J. Van Der Ent, R. Woods, and H. H. G. Savenije, 2012: An analytical model for soil-atmosphere feedback. *Hydrol. Earth Syst. Sci.*, **16**, 1863–1878, https://doi.org/10.5194/hess-16-1863-2012.

Schär, C., and Coauthors, 2016: Percentile indices for assessing changes in heavy precipitation events. *Climatic Change*, **137**, 201–216, https://doi.org/10.1007/s10584-016-1669-2.

——, and Coauthors, 2020: Kilometer-scale climate models: Prospects and challenges. *Bull. Amer. Meteor. Soc.*, **101**, E567–E587, https://doi.org/10.1175/BAMS-D-18-0167.1.

Schubert-Frisius, M., F. Feser, H. von Storch, and S. Rast, 2017: Optimal spectral nudging for global dynamic downscaling. *Mon. Wea. Rev.*, **145**, 909–927, https://doi.org/10.1175/MWR-D-16-0036.1.

Separovic, L., R. de Elía, and R. Laprise, 2012: Impact of spectral nudging and domain size in studies of RCM response to parameter modification. *Climate Dyn.*, **38**, 1325–1343, https://doi.org/10.1007/s00382-011-1072-7.

Takayabu, I., and Coauthors, 2022: Convection-permitting models for climate research. *Bull. Amer. Meteor. Soc.*, **103**, E77–E82, https://doi.org/10.1175/BAMS-D-21-0043.1.

Tang, J., X. Sun, P. Hui, Y. Li, Q. Zhang, and J. Liu, 2018: Effects of spectral nudging on precipitation extremes and diurnal cycle over CORDEX-East Asia domain. *Int. J. Climatol.*, **38**, 4903–4923, https://doi.org/10.1002/joc.5706.

Taylor, C. M., R. A. M. de Jeu, F. Guichard, P. P. Harris, and W. A. Dorigo, 2012: Afternoon rain more likely over drier soils. *Nature*, **489**, 423–426, https://doi.org/10.1038/nature11377.

Teufel, B., and Coauthors, 2017: Investigation of the 2013 Alberta flood from weather and climate perspectives. *Climate Dyn.*, **48**, 2881–2899, https://doi.org/10.1007/s00382-016-3239-8.

Tremblay, M., and C. Guillaud, 2019: The 1996 Saguenay flood event and its impacts. *Nat. Hazards*, **98**, 79–89, https://doi.org/10.1007/s11069-018-3494-6.

Uber, M., J.-P. Vandervaere, I. Zin, I. Braud, M. Heistermann, C. Legoût, G. Molinié, and G. Nord, 2018: How does initial soil moisture influence the hydrological response? A case study from southern France. *Hydrol. Earth Syst. Sci.*, **22**, 6127–6146, https://doi.org/10.5194/hess-22-6127-2018.

United Nations Department of Economic and Social Affairs, 2024: The Sustainable Development Goals Report 2024. UN DESA Rep., 51 pp., https://unstats.un.org/sdgs/report/2024/.

Verseghy, D. L., 1991: Class—A Canadian land surface scheme for GCMS. I. Soil model. *Int. J. Climatol.*, **11**, 111–133, https://doi.org/10.1002/joc.3370110202.

——, 2000: The Canadian Land Surface Scheme (CLASS): Its history and future. *Atmos.–Ocean*, **38**, 1–13, https://doi.org/10.1080/07055900.2000.9649637.

von Storch, H., H. Langenberg, and F. Feser, 2000: A spectral nudging technique for dynamical downscaling purposes. *Mon. Wea. Rev.*, **128**, 3664–3673, https://doi.org/10.1175/1520-0493(2000)128<3664:ASNTFD>2.0.CO;2.

Warren, F., and N. Lulham, Eds., 2021: Canada in a Changing Climate: National Issues Report. Government of Canada Rep., 734 pp., https://www.cakex.org/sites/default/files/documents/National-Issues-Report_Final_EN.pdf.

Wei, J., H. Su, and Z.-L. Yang, 2016: Impact of moisture flux convergence and soil moisture on precipitation: A case study for the southern United States with implications for the globe. *Climate Dyn.*, **46**, 467–481, https://doi.org/10.1007/s00382-015-2593-2.

Zadra, A., D. Caya, J. Côté, B. Dugas, C. Jones, R. Laprise, K. Winger, and L.-P. Caron, 2008: The next Canadian regional climate model. *Phys. Can.*, **64**, 75–83.